EDGEWOOD CHEMICAL BIOLOGICAL CENTER
U.S. ARMY RESEARCH, DEVELOPMENT AND ENGINEERING COMMAND
Aberdeen Proving Ground, MD 21010-5424

ECBC-TR-1243

SPECTRAL CHARACTERIZATION OF RDX, ETN, PETN, TATP, HMTD, HMX, AND C-4 IN THE MID-INFRARED REGION

Clayton S.C. Yang

BATTELLE EASTERN SCIENCE AND TECHNOLOGY CENTER
Aberdeen, MD 21001-1228

Barry R. Williams
Ashish Tripathi
Melissa S. Hulet

LEIDOS
Gunpowder, MD 21010-0068

Alan C. Samuels
Joseph A. Domanico
Joseph May
Ronald W. Miles, Jr.
Augustus W. Fountain III

RESEARCH AND TECHNOLOGY DIRECTORATE

April 2014

Disclaimer

The findings in this report are not to be construed as an official Department of the Army position unless so designated by other authorizing documents.

REPORT DOCUMENTATION PAGE

Form Approved
OMB No. 0704-0188

1. REPORT DATE *(DD-MM-YYYY)*	2. REPORT TYPE	3. DATES COVERED *(From - To)*
XX-04-2014	Final	Aug 2012 - Oct 2013

4. TITLE AND SUBTITLE
Spectral Characterization of RDX, ETN, PETN, TATP, HMTD, HMX, and C-4 in the Mid-Infrared Region

5a. CONTRACT NUMBER

5b. GRANT NUMBER

5c. PROGRAM ELEMENT NUMBER

6. AUTHOR(S)
Yang, Clayton S.C. (BEST); Williams, Barry R.; Tripathi, Ashish; Hulet, Melissa S. (Leidos); Samuels, Alan C.; Domanico, Joseph A.; May, Joseph; Miles, Ronald W., Jr.; and Fountain, Augustus W. III (ECBC)

5d. PROJECT NUMBER
(DHS IAA) 1210G [HSHQPM-12-X-00017]

5e. TASK NUMBER

5f. WORK UNIT NUMBER

7. PERFORMING ORGANIZATION NAME(S) AND ADDRESS(ES)
Battelle Eastern Science and Technology Center, 1204 Technology Drive, Aberdeen, MD 21001-1228
*Leidos, P.O. Box 68, Gunpowder, MD 21010-0068
Director, ECBC, ATTN: RDCB-DRD-P, Aberdeen Proving Ground, MD 21010-5424

8. PERFORMING ORGANIZATION REPORT NUMBER
ECBC-TR-1243

9. SPONSORING / MONITORING AGENCY NAME(S) AND ADDRESS(ES)
Department of Homeland Security, 245 Murray Lane SW, Washington DC 20528-0075

10. SPONSOR/MONITOR'S ACRONYM(S)
DHS

11. SPONSOR/MONITOR'S REPORT NUMBER(S)

12. DISTRIBUTION / AVAILABILITY STATEMENT
Approved for public release; distribution is unlimited.

13. SUPPLEMENTARY NOTES
*Science Applications International Corporation changed its name to Leidos on September 27, 2013.

14. ABSTRACT
We report on the complex optical constants (*n* and *k*) of RDX, ETN, PETN, TATP, HMTD, HMX, and C-4 as determined by variable angle spectroscopic ellipsometry (VASE) over the mid-infrared (MIR) wavelength range from 2.5 to 16.7 μm (4000 to 600 cm^{-1}). The samples were prepared for analysis by airbrushing onto a zinc selenide (ZnSe) crystal and then analyzed in attenuated total reflection (ATR) mode. The optical constants of HMX and RDX are compared with previously reported values. No previously reported studies of the optical constants of ETN, PETN, TATP, and C-4 were found in the literature.

15. SUBJECT TERMS
Absorptivity coefficient; Attenuated total reflection (ATR); Fourier transform infrared (FTIR); Refractive index; Imaginary index of refraction; Real index of refraction; Variable angle spectroscopic ellipsometry (VASE); Explosive; Energetic; Mid-infrared; RDX; HMX; HMTD; ETN; PETN; TATP; C-4

16. SECURITY CLASSIFICATION OF:			17. LIMITATION OF ABSTRACT	18. NUMBER OF PAGES	19a. NAME OF RESPONSIBLE PERSON
					Renu B. Rastogi
a. REPORT	b. ABSTRACT	c. THIS PAGE			19b. TELEPHONE NUMBER
U	U	U	UU	50	(410) 436-7545

BLANK

PREFACE

The work described in this report was performed in support of the Department of Homeland Security under Inter-Agency Agreement Number (DHS IAA) 1210G [HSHQPM-12-X-00017]. This work was started in August 2012 and completed in October 2013.

The use of either trade or manufacturers' names in this report does not constitute an official endorsement of any commercial products. This report may not be cited for purposes of advertisement.

This report has been approved for public release.

Acknowledgments

The authors thank Drs. Avishai Ben-David (U.S. Army Edgewood Chemical Biological Center) and Charles Davidson (Science and Technology Corporation, Edgewood, MD) for their helpful discussions of the approach used to validate the ellipsometry methods.

BLANK

CONTENTS

LIST OF FIGURES

LIST OF TABLES

ACRONYMS AND ABBREVIATIONS

ACN	Acetonitrile
ATR	Attenuated total reflection
C-4	Composite C (explosive comprised of RDX and binder)
DMDNB	2,3-Dimethyl-2,3-dinitrobutane
EBAD	Ensign Bickford Aerospace & Defense Company
ECBC	Edgewood Chemical Biological Center
ETN	Erythritol tetranitrate
FTIR	Fourier transform infrared spectroscopy
HAAP	Holston Army Ammunition Plant
HMTD	Hexamethylene triperoxide
HMX	Cyclotrimethylene tetranitrate
IED	Improvised explosive device
IR	Infrared
IRE	Internal reflection element
K	Linear absorption coefficient
k	Absorption index/Extinction coefficient
K-K	Kramers-Kronig
KBr	Potassium Bromide
LC	Liquid chromatography
MIR	Mid-infrared
n	Real refractive index
PBA	Poly(1,4-butylene adipate)
PETN	Pentaerythritol tetranitrate
PIB	Poly(isobutylene)
PMMA	Poly(methyl methacrylate)
RCE	Rotating-compensator ellipsometer
RDX	Cyclotrimethylenetrinitramine
TATP	Triacetone triperoxide
VASE	Variable angle spectral ellipsometry
ZnSe	Zinc selenide

BLANK

ABSTRACT

We report the complex optical constants (*n* and *k*) of erythritol tetranitrate (ETN), hexamethylene triperoxide diamine (HMTD), cyclotetramethylene tetranitramine (HMX), pentaerythritol tetranitrate (PETN), cyclotetramethylene tetranitramine (RDX), triacetone triperoxide (TATP), and Composite C (C-4) explosives as determined by variable angle spectroscopic ellipsometry (VASE) over the mid-infrared (MIR) wavelength range from 2.5 to 16.7 μm (4000 to 600 cm^{-1}). The samples were prepared for analysis by airbrushing onto a zinc selenide (ZnSe) crystal, which were then analyzed in attenuated total reflection (ATR) mode. The optical constants of HMX and RDX are compared with previously reported values. No previously reported studies of the optical constants of ETN, PETN, TATP, and C-4 were found in the literature.

BLANK

SPECTRAL CHARACTERIZATION OF RDX, ETN, PETN, TATP, HMTD, HMX, AND C-4 IN THE MID-INFRARED REGION

1 INTRODUCTION

Due to concerns related to homeland security and defense, fast and effective detection of energetic materials is an active area of research. Efficient and reliable detection systems are especially needed at airports, transportation terminals, and national security sites and events. The nature of the threat from explosives includes not only commercially-produced materials and munitions, but also improvised explosive devices (IED). The explosives used in IEDs may be synthesized from common domestic chemicals, such as the triacetone triperoxide (TATP), which was used in the London public transport bombings.1 The development of sensitive optical methods to detect these substances is critical for implementing faster and less invasive screening procedures.

For isotropic materials, including most of the explosive organic compounds, one complex parameter, the index of refraction ($\tilde{n}$ =*n*+*ik*), is sufficient to describe the response of these materials to external optical (electromagnetic) fields. The optical constants *n* and *k* represent the optical properties of a material in terms of how an electromagnetic wave will propagate in the material.* The value *n,* the real index of refraction, is related to the phase change of the applied electromagnetic field due to the light-material interaction. The value *k*, the extinction coefficient (or absorption index), is proportional to the degree to which the applied electromagnetic field is attenuated by absorption in the material. If the optical constants are known, one can accurately predict the intensity of the reflected and/or transmitted light through the bulk materials. The infrared (IR) spectrum in the mid-infrared (MIR) region has long been used for compound identification and structure classification. Given the optical constants of target materials in the MIR region, the performance of a stand-off MIR optical explosive sensor may be assessed for a range of arbitrary circumstances.

Traditionally the optical constants in the MIR region have been investigated via transmission techniques. Methods have been refined to correct thin film spectra of liquids in short path cells for the effects such as Fresnel reflection from the windows of the cells and the optical dispersion of the liquid being measured.2-5 The method yields the linear absorption coefficient (*K*), which describes the absorbance in a material per unit of length. This can then be used to compute the dimensionless absorption index (*k*), the imaginary part of the complex refractive index, where $\tilde{\nu}$ is the reciprocal of the wavelength in centimeters:

$$k(\tilde{\nu}) = \frac{\ln(10)K(\tilde{\nu})}{4\pi\tilde{\nu}} \quad (1)$$

* In the literature, the imaginary part of the complex refractive index, *ik*, is usually shortened to *k* when not used in equation form with the real refractive index. That is the convention used in this report. The complex refractive index should not be confused with the linear absorption coefficient, which describes absorbance in a material per unit of length. The relationship between *k* and *K* is described as: $K = \frac{4\pi k\tilde{\nu}}{\ln(10)}$, where $\tilde{\nu}$ is the reciprocal of the wavelength in centimeters for absorbance computed as the common logarithm of transmittance.

The imaginary refractive index is then mathematically manipulated through a Kramers-Kronig (K-K) transformation to derive the real part (n) of the optical constants that are required to model standoff detection performance.

$$n(\tilde{\nu}_i) = \frac{2}{\pi} P \int_0^{\infty} \frac{\nu k(\tilde{\nu})}{\nu^2 - \nu_i^2} \, d\nu + n(\infty) \qquad (2)$$

The term, $n(\infty)$, which is the real refractive index at infinity, is not available. For that reason, Equation 2 has been evaluated by using an anchor point of n that is as close as possible to the highest wavenumber value of the measured spectral range. For many materials, measured values of n are available only at the sodium-D line of 589.3 nm, well outside of the MIR range. Other pitfalls can present themselves when a K-K relationship is used to derive the real part of the complex refractive index. Nonzero values of k outside the range being evaluated can cause the calculated values of n to be skewed from the true values, particularly when peaks in k are just outside the measured range.6 Finally, Equation 2 includes a pole where $v = v_i$ and can only be approximated around the pole.

IR spectroscopic ellipsometry has been proven to be superior to other IR spectroscopic means of determining the complex index of refraction of isotropic condensed phase materials, as both optical constants of the complex index of refraction can be determined in a single ellipsometric measurement without the need for mathematical transformation and data extrapolation outside the spectral range.[7-8] Ellipsometry is self-sufficient in the sense that no reference measurement is necessary. The accuracy of optical constants measurements is greatly enhanced because of not only the absolute intensity of the reflected light, but the relative change of both the intensity and phase between different polarizations of the reflected light is measured in ellipsometry.

We have previously demonstrated that attenuated total reflectance infrared (ATR-IR) spectroscopic ellipsometry, which has been used to measure the optical constants of a variety of organic liquids, is an appropriate probe for the measurement of n and k of liquid compounds, including highly toxic chemical warfare agents.[6,9-11] Further validation of the technique was achieved by comparing the optical constants of benzene and toluene generated in our laboratory using ATR-IR spectroscopic ellipsometry to high quality literature data.[12-13] Spectra of the compounds at several different resolutions were also used to assess the effects of the limited resolution (4 cm^{-1}), at which the spectra of nearly all the materials were measured. Both compounds showed an excellent correlation with the literature. Figure 1 shows the complex optical constants of toluene from ellipsometry measurements and the literature study,[13] which demonstrated that the experimental spectra give a good correlation with the reference data. Agreement between the ATR-IR ellipsometry and reference spectra was excellent across nearly the full spectral range, although a few strong, very narrow bands exhibited slight increases in their peak maxima at higher resolution. This demonstrated that the optical properties of materials in the IR region can be readily and accurately measured by ATR-IR ellipsometry without the need for more involved experimental and mathematical approaches.

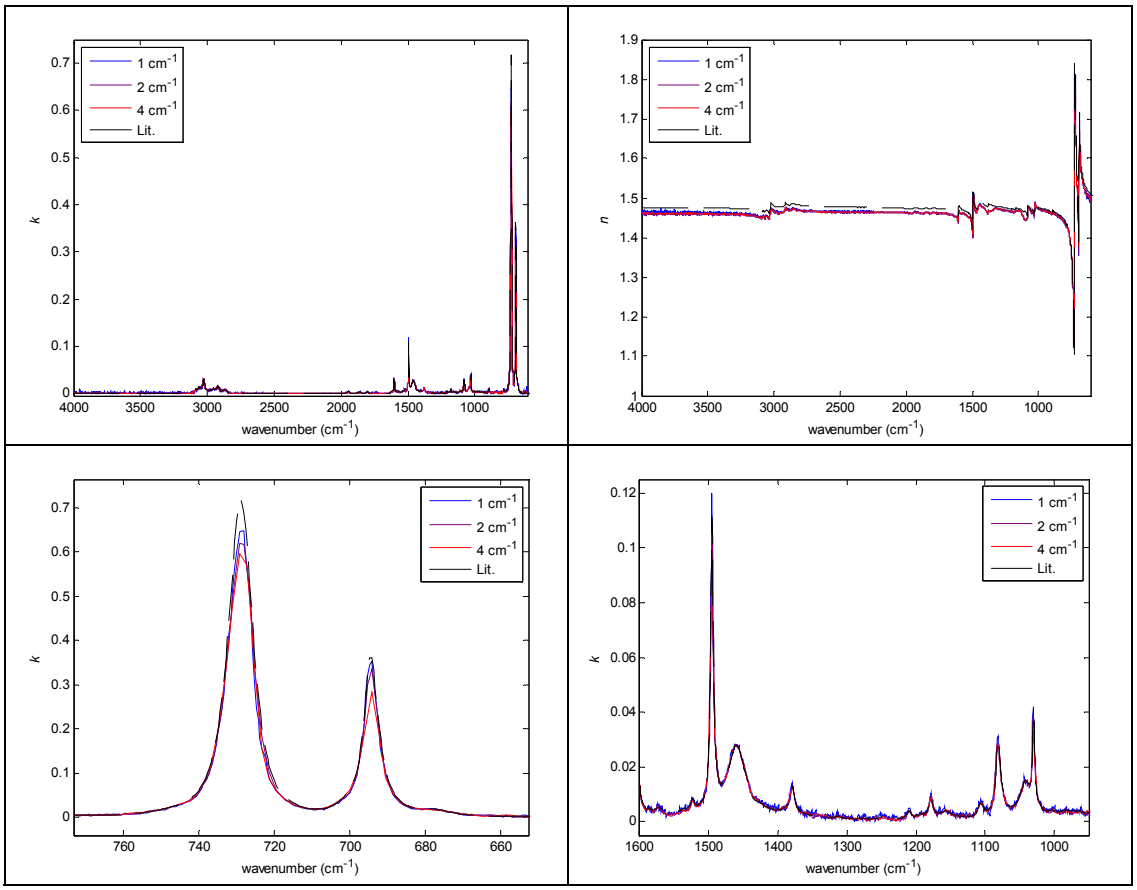

Figure 1. Top: Complex optical constants of toluene: k (left); n (right). Bottom: Expanded views of regions in the k-spectrum (left and right). Legends contain the spectral resolution of the ATR-IR ellipsometry data.

Besides the conventional IR spectroscopic measurements of powder samples, attenuated total reflectance Fourier transform infrared spectroscopy (ATR-FTIR) has been used for surface analysis of powder mixtures.6 ATR-FTIR presents potential advantages over many *in situ* powder probing methods, as it requires minimal sample preparation and is effective with fine-grained materials. The sample of interest is placed in close physical contact with a crystal of high refractive index, such as zinc selenide (ZnSe), germanium, or diamond. Modulated IR light from a Fourier transform infrared (FTIR) interferometer enters the crystal at such an angle that when the light hits the interface with the sample, total internal reflection occurs. Light penetrates the sample via an evanescent wave that rapidly decays away from the interface. The beam is attenuated at frequencies corresponding to the fundamental vibrational modes and overtones of the sample. The resultant ATR spectrum has peak positions similar to those in an equivalent transmission IR spectrum in the literature. In the present study, we broadened our measurement techniques to apply ATR-FTIR ellipsometry to investigate the optical properties of solid energetic materials in the MIR region.

2 METHODS AND MATERIALS

2.1 Infrared Spectroscopic Ellipsometry

Ellipsometry is commonly used to characterize both thin film and bulk materials. The typical experimental setup of an ellipsometer consists of a light source, a pair of linear polarizers and a compensator, usually a quarter-wave plate as shown in Figure 2.

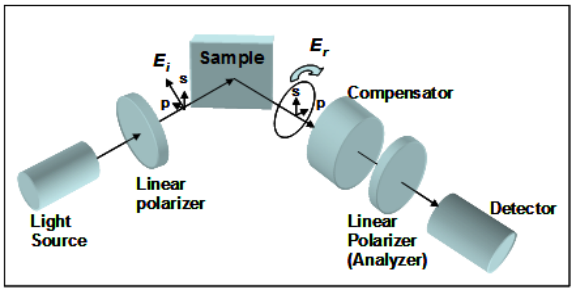

Figure 2. Typical experimental setup of an ellipsometer.

Plane polarized light is reflected from the sample surface to produce an elliptically polarized reflected light. Ellipsometry measures the change in polarization state (intensity and phase) of light reflected from the surface of a material. The actual measurements given by an ellipsometer are the values ψ and Δ, which are commonly referred to as the ellipsometric parameters. These two real-number values are related to the ratio of complex Fresnel reflection coefficients R_p and R_s, for *p*- and *s*- polarized light respectively by:[10]

$$\tan\psi \exp(i\Delta) = \frac{R_p}{R_s} = \rho \quad , \textit{i.e.}, \tag{3}$$

$$\psi = \tan^{-1}\frac{|R_p|}{|R_s|} \; ; \; \Delta = \delta_p - \delta_s = (\arg\, r_p - \arg\, r_s) \tag{4}$$

where $\tan\psi$ equals to the ratio of reflectivity amplitude. Geometrically, ψ can be interpreted as the angle between the two axes of the reflected polarization ellipse and the linear polarization direction of the incident beam. The other ellipsometric parameter, Δ, is related to the ratio of the polarization ellipse's main axes. Physically, it is the measure of a phase shift between *s*- and *p*- components of the light due to the reflection off the sample.

The Fresnel reflection coefficients for an interface of two media (e.g., medium 0 and medium 1) are:[11]

$$R_p = R_{01p} = \frac{N_1\cos\theta_0 - N_0\cos\theta_1}{N_1\cos\theta_0 + N_0\cos\theta_1} \quad (\text{for } p \text{ polarized light}) \tag{5}$$

$$R_s = R_{01s} = \frac{N_0\cos\theta_0 - N_1\cos\theta_1}{N_0\cos\theta_0 + N_1\cos\theta_1} \quad (\text{for } s \text{ polarized light}) \tag{6}$$

where λ and θ_0 are generally known quantities, N_0 can be measured independently, and θ_1 is a related to N_0 and N_1 through Snell's law. Therefore, from the ratio of effective Fresnel

coefficients ($R_{p,s}$) acquired from ellipsometry measurement, one can determine the optical constant of the target material (N_1).

The ellipsometer in our laboratory, the infrared variable angle spectroscopic ellipsometer (IR-VASE), is a rotating-compensator ellipsometer (RCE). The RCE provides an improved automatic capability to unambiguously determine the elliptical polarization phase angle Δ in a single measurement. In the RCE, both polarizing elements, the polarizer and analyzer, are fixed at 45° and 0°, respectively, and a quarter-wave retardation element placed in the path of the light beam is continuously rotated. The intensity of the detector signal is monitored as a function of instantaneous rotational angles of the rotating retarder (compensator):8

$$I_D \propto 1 + \frac{2\sin 2\psi \sin \Delta}{2 - \cos 2\psi}\sin(2A) - \frac{\cos 2\psi}{2 - \cos 2\psi}\cos(4A) + \frac{\sin 2\psi \cos \Delta}{2 - \cos 2\psi}\sin(4A) \qquad (7)$$

where I_D is the intensity of the IR beam at the detector and A is the compensator angle. The presence of both $\sin\Delta$ and $\cos\Delta$ terms in the coefficients of the FTIR-analyzed RCE measured signal permits Δ to be unambiguously determined with higher accuracy.

2.2 Vertical Attenuated Total Reflectance Infrared Variable Angle Spectroscopic Ellipsometry

The experimental setup described in Section 2.1 is suitable for probing the complex optical constants of solids if they can be obtained or prepared as a single slab or crystal with a very high degree of smoothness. We were able to achieve this for a few materials by pressing pellets of the pure compounds at about 9 to 10 tons/in². The majority of compounds, however, proved unsuitable because they were too reactive, were too friable in pellet form, or (in the case of Composite C (C-4)) were composites. For this reason, we investigated a method of adapting the vertical ATR IR-VASE technique that had been used to measure the complex optical constants of liquids.[6,10] The ATR sampling assembly consisted of a stainless steel holder, an ATR crystal, and a multi-dimensional alignment stage (Figure 3). This sampling assembly was vertically mounted onto the high precision θ - 2θ sample rotational stage of the IR-VASE. For the sake of simplicity, the ATR crystal that was used in this study was a 45° ZnSe prism. The faces of the prism that coupled to the optical path of the ellipsometer were anti-reflection coated, whereas the face that comes into contact with the sample under study was uncoated. The explosive sample powders needed to be deposited onto the uncoated surface of the crystal in a uniform thin film. The ATR crystal was affixed to the holder with a stainless steel bar. The sampling assembly was vertically mounted on a sample stage in the IR-VASE ellipsometer. A laser alignment assembly of the IR-VASE and the ATR assembly multi-dimension stage were used together to ensure that the rotational axis of the ATR assembly was on the sample film-ATR crystal interfacial plane, perpendicular to the plane of incidence, and intersecting both incident and reflected IR beams on the ATR-sample interface.

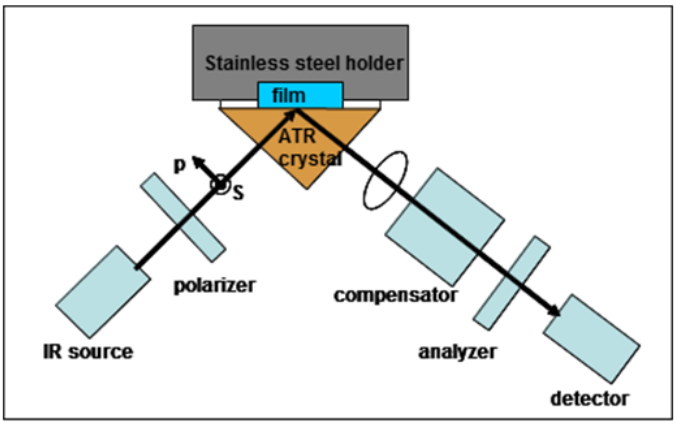

Figure 3. Experimental setup of our IR-VASE ellipsometer with a vertical ATR assembly.

The ATR assembly setup must be calibrated prior to each measurement of the optical properties of sample compounds. This calibration procedure aimed to determine the optical properties (especially birefringence) of the ATR crystal, which can be effectively represented by a model with a couple of independent fitting parameters. The calibration was performed with no sample deposited on the back of the ATR crystal. Incorporating the calibration parameters that characterize the birefringence of the ATR crystal into the Fresnel model of the ATR crystal-sample film interface greatly improves the accuracy of the optical constant measurements of the sample film. Therefore, the resolution of the calibration was the same as that of the sample measurement: 4 cm^{-1} in this study. The calibration data were computed as the mean of two spectra (from 10 co-added scans each) at a 45° incident angle. Additional instrument parameters are shown in Table 1.

Table 1. Instrument parameters used in ellipsometry measurements.

Setting	Value
Resolution	4 cm^{-1}
Zero-fill	2
Final data spacing	2 cm^{-1}
Spectra/Rev	15
Scan/Spectrum	20
Measure/Cycles/Angle	10
Bandwidth	0.02 μm
Minimum Intensity ratio	2 to 5
Sample Type	Isotropic
Input Polarizer	45° with Zone Averaging
RCE Analyzer	Single Position

2.3 Preparation of Thin Films

We initially investigated two methods of getting the explosive compounds to form thin films on the surface of the ZnSe crystal. In the first attempt, the powdered compounds were physically pressed on the crystal using a stainless steel piston that screwed into the body of the holder. That method proved entirely unsatisfactory for two reasons. First, when measured, the Ψ and Δ resulted in optical constants that were essentially identical to air, which indicated that,

at least within the ATR depth of penetration, there were large voids within the samples. Second, the pressure of the piston on the ZnSe crystal induced a high degree of birefringence on the crystal that was difficult to correct. Next, we attempted to generate uniform films of the target compounds on the ZnSe crystal by evaporating solutions directly onto the uncoated face of the crystal. Again we found that the data indicated that the samples seemingly contained large voids that rendered the data unusable.

The approach for preparing thin films of the materials that ultimately proved useful was an airbrush technique. Solutions of the target materials were either obtained from commercial sources or prepared by diluting the neat material in solvent. Concentrations of the solutions ranged from 5 to 40 mg/mL, depending upon the availability of commercial solutions or the solubility of the material in the solvent. We found that heating the prism gently during deposition to evaporate the solvent carrier as rapidly as possible after the aerosolized droplets impacted the sample surface of the crystal improved the quality of the resulting film. We coordinated with the Advanced Design and Manufacturing Branch at Edgewood Chemical Biological Center (ECBC) to fabricate a copper holder for the prism. The copper holder was set on a 12 in^2 heating pad that rested on a 12 in^2 ceramic tile. During airbrushing, the assembly was heated to a temperature approximately 20°C below the boiling point of the solvent (or lower if the material was unstable at that temperature). An aluminum mask was placed over the uncoated sample side of the prism to minimize transfer of the spray to the anti-reflection coated faces of the prism. Photographs of the prism, mask, and heater assembly are shown in Figure 4. Also shown in the figure is a photograph of the uncoated sample face of a prism after airbrushing a thin film of a compound. With the exception of isolated clusters of diffusely reflecting crystals of the analyte at the surface, the thin film on the crystal is clear.

Preparing thin, homogeneous films of the materials required a combination of science and art. First, the solvent needed to be compatible with the components of the airbrush. This excluded chlorinated solvents, such as dichloromethane. Second, the target compound needed to have sufficient solubility in the solvent to prepare a solution of at least several milligrams per milliliter. Finally, the boiling point of the solvent needed to be high enough that the aerosolized droplets from the spray impacted the crystal in a liquid state, followed by rapid evaporation of the solvent carrier to form a crystalline film of the energetic materials. Acetonitrile (ACN) was found to give the best combination of solvent properties. Combinations of two or more solvents were used in some cases, and solvents and concentrations of target compounds were often adjusted on a trial and error basis to achieve a uniform thin film on the sample face of the prism.

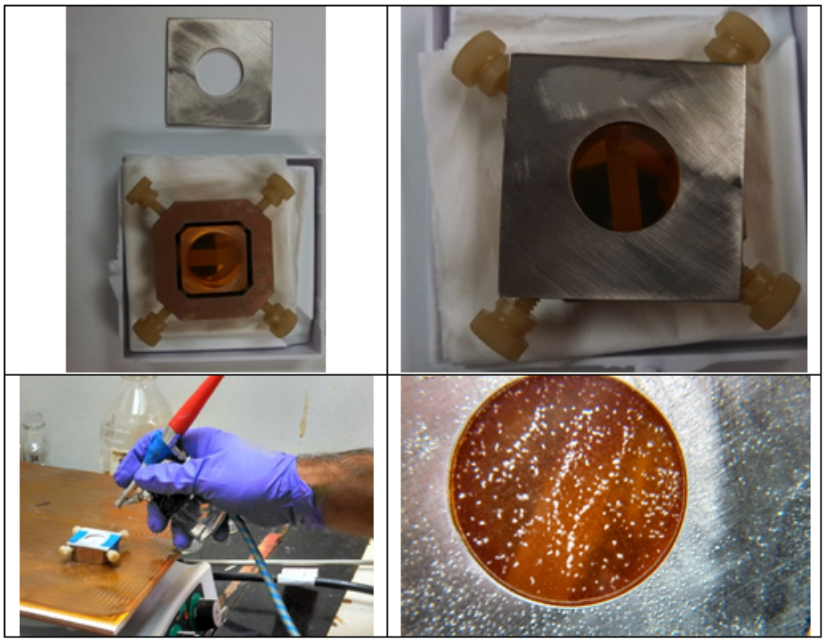

Figure 4. Top: ATR prism in copper holder and aluminum mask (left); prism and holder with aluminum mask in place over the uncoated face of the prism (right). Bottom: Airbrushing the prism while it rested on the heater assembly. The blue masking tape is also shown holding the mask in place to further protect the anti-reflection coated faces of the prism (left); the ZnSe crystal after airbrushing (right).

To protect the operator, all airbrushing was done in a fume hood. The spray was adjusted until the aerosolized conical spray from the nozzle of the airbrush was nearly invisible to the naked eye. The spray was then applied to the surface of the prism in a sweeping motion for several seconds, with the nozzle tip at a distance of 5 to 10 cm from the surface. The crystal was then rotated 90° and additional material was applied. This was repeated until all the volume (approximately 20 mL) of the liquid reservoir had been applied.

At a 45° angle of incidence with a ZnSe prism, the maximum ATR depth of penetration was <20 μm at the longest wavelengths in our study. The thin crystalline films that were produced adhered to the surface readily, apparently through Van der Waals forces. Films much thicker than the maximum depth of penetration sometimes delaminated and were thus undesirable.

After spraying, crystalline film on the surface of the prism was visually inspected. An ideal film was nearly transparent and continuous, with no gaps, and had only a slightly diffusely reflecting top surface. The prism was removed from the holder, the anti-reflection coated surfaces were gently cleaned with lens paper and solvent to remove any traces of contamination from the spray, and the prism was mounted in the stainless steel holder for measurement on the ellipsometer. To acquire ellipsometric data of the tested film, we took 20 scans per spectrum and averaged 20 spectra at 45° incident angle while setting the resolution of the measurement to be 4 cm^{-1}. The measured ellipsometric parameters (ψ and Δ) of the ATR crystal-sample film system were used to determine optical constants of the films. Since ellipsometry is a non-contact optical modulation technique, sample damage is a non-issue and baseline scans or reference samples are not required. For the purposes of this study, the optical constants (*n* and *k*) of the films were determined over a wide MIR wavelength range from 2.5 to 16.7 μm (4000 to 600 cm^{-1}). Usually at least one additional layer of material was then applied by

airbrushing onto the existing film on the surface of the prism, which was re-measured until the response (Ψ and Δ) was stable.

The MIR optical constants of a few solid organic compounds, primarily polymers, have been reported in the literature. Allara, et al.,[14] investigated the *n* and *k* of poly(methyl methacrylate) (PMMA), limited to the carbonyl region only, using reflection spectra of thin films of the polymer on gold and silicon substrates. Graf, et al., [15] determined the optical constants in a broader spectral range using transmission spectra of cast films and a K-K transformation and showed that their optical constants were "very similar" to those reported by Allara, at least within the limited spectral range of that study. Therefore, we selected PMMA for analysis by ATR-VASE using the airbrush technique to prepare a thin film of the polymer. A solution of PMMA (Sigma-Aldrich; Cat. No. 182230, average M.W. 120,000) was prepared at a concentration of 5 mg/mL in ACN. The solution was airbrushed onto the ZnSe prism, followed by measurement of the thin film ATR-VASE, a total of three times. The Ψ spectrum showed little or no change after the second application of the polymer, while the Δ spectrum exhibited only a very small change near the low frequency end of the measurement range. The *k* values computed from the ATR-VASE measurements were very similar to those obtained by Graf, et al. The real refractive index from the ATR-VASE measurements was approximately 3% higher than the literature values near 3500 cm^{-1}, with the values converging near the low frequency end of the range, where there was little or no difference. Figure 5 shows the raw data (Ψ and Δ) from our measurements, along with a comparison of the optical constants from ATR-VASE to the values in the literature (digitized from Graf, *et. al*.[15]).

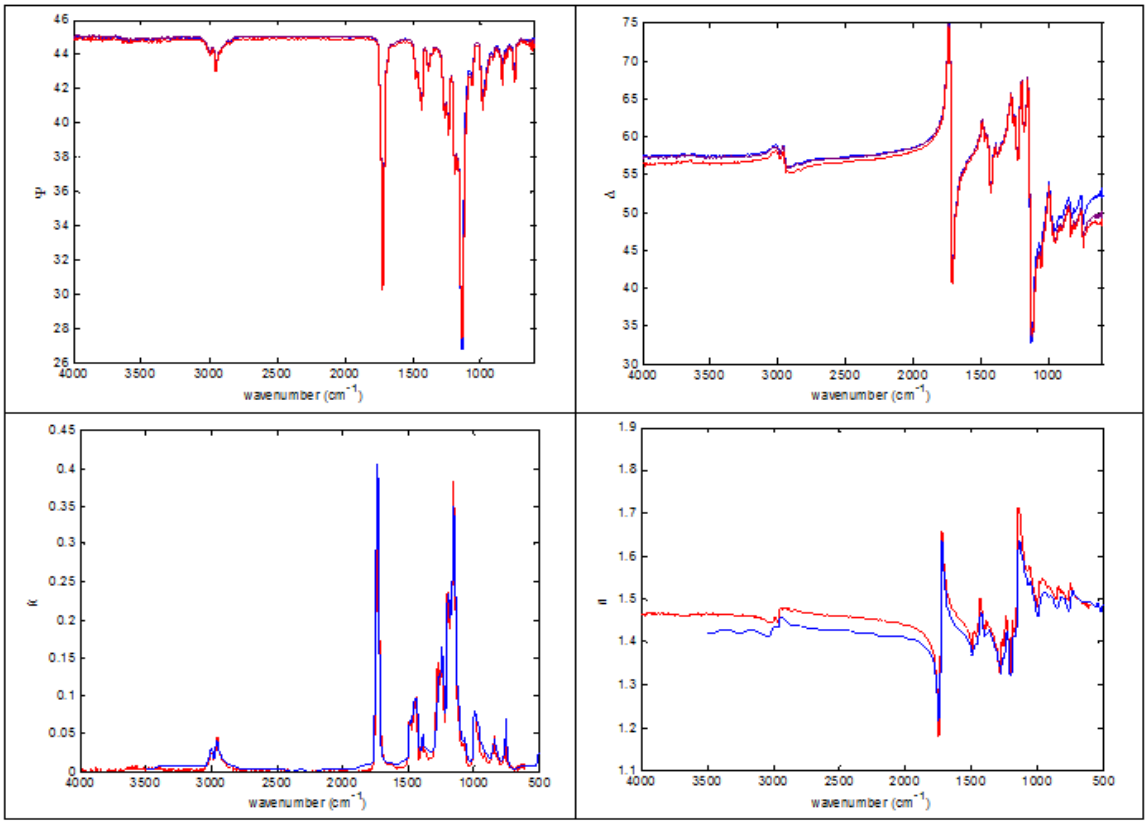

Figure 5. Top: Ψ and Δ (left and right, respectively) from three successive applications of PMMA solution onto a ZnSe prism. Bottom: Computed optical constants from ATR-VASE (in red) and digitized from the literature[15] (in blue).

2.4 Fourier Transform Infrared-Attenuated Total Reflection Measurements

Some materials were also run by FTIR-ATR spectroscopy using a Thermo-Nicolet (Madison, WI) 670 FTIR spectrometer that was equipped with a GoldenGate ATR accessory with a diamond internal reflection element (IRE). Detailed instrument parameters are given in Table 2.

Table 2. Instrument parameters for Thermo-Nicolet 670 FTIR spectrometer.

Setting	Value
Number of background scans	64
Number of sample scans	64
Resolution	4 cm^{-1}
Zero-filling	2
Apodization	Happ-Genzel
Phase correction	Mertz
Spectral range (cm^{-1})	4000-650
Final data spacing	1.928 cm^{-1}
Detector	MCT/A
Optical velocity (cm/s)	1.898
Aperture	69

Because both ATR-VASE and FTIR-ATR spectrometry are ATR techniques, they tend to yield spectra that are similar in appearance.[†] The depth of penetration of the evanescent wave in both techniques is proportional to the wavelength and dependent upon the difference between the refractive index of the sample and IRE. The refractive index of diamond ($n_{10\mu m}$=2.38) is similar to that of ZnSe ($n_{10\mu m}$=2.41), although the dispersion curve of ZnSe exhibits a sharper decrease at wavelengths greater than 10 μm.[16] The angle of incidence in the GoldenGate is fixed at 45°, which is the same as that used in our ATR-VASE method. This made FTIR-ATR useful for quickly and easily acquiring spectra of the C-4 variants for comparison to one another and elucidating differences in the formulations. Diamond absorbs strongly within approximately 2500-1900 cm^{-1}, which tends to induce noise within the region. The *straightline* function in the Omnic software was used to improve the appearance of the spectrum and improve the results of search algorithms. Spectra were also subjected to a multipoint linear baseline correction. In addition, any FTIR-ATR spectrum that was searched using the Aldrich Library of FTIR Spectra[17] was first subjected to the Omnic Advanced ATR Correction to yield a spectrum more similar to a transmission spectrum.

[†] Although both techniques employ attenuated total reflection, for reasons of clarity and brevity, we use ATR-VASE to refer to the ellipsometer and FTIR-ATR to refer to the Thermo-Nicolet 670 and GoldenGate accessory (or the data acquired from the respective instruments) for the remainder of this report.

2.5 Materials

Production and distribution of explosives is highly regulated by United States (U.S.) federal law. With the exception of TATP, which was supplied by the Explosive Ordnance Laboratory at the Naval Surface Warfare Center at Indian Head, Maryland, the materials in this study were obtained through the Explosives and Pyrotechnics Branch at ECBC. Personnel at both facilities are highly knowledgeable and experienced in the physical and chemical properties, as well as the safety considerations applicable to the handling of energetic materials. Of the materials provided through the Explosives and Pyrotechnics Branch, erythritol tetranitrate (ETN) and hexamethylene triperoxide diamine (HMTD) were obtained in solution from a commercial source (Accustandard, New Haven, CT) at a concentration of 5 mg/mL; and pentaerythritol tetranitrate (PETN) and cyclotetramethylene tetranitramine (RDX) were cut from Primacord (100 gr/ft). Samples from varying lots of C-4 had been manufactured by Holston Army Ammunition Plant (HAAP) (Kingsport, TN). The sample used to obtain the optical constants was from a custom batch that had been manufactured without taggant. Properties and structures of the materials studied are given in Table 3.

Table 3. Structures and physical properties of the chemical agents studied for this report.

Properties	Structure
Name: Composite C (C-4) FW: Various Lot: Various (see note at bottom of table) Source: Holston Army Ammunition Plant	Multiple
Name: Erythritol tetranitrate (ETN) Formula: $C_4H_6N_4O_{12}$ FW: 302.11 Density (g/cm^3): 1.6 Source: AccuStandard, S-2001Q-5X, 5 mg/mL in acetonitrile Lot: 21305127	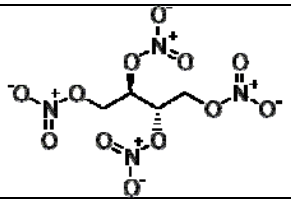
Name: Hexamethylene triperoxide diamine (HMTD) CAS RN: 283-66-9 Formula: $C_6H_{12}N_2O_6$ FW: 208.17 Density (g/cm^3): 0.88 Source: Accustandard, S-2001L, 5 mg/mL in acetonitrile Lot: 213051374	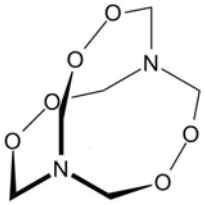
Name: Cyclotetramethylene-tetranitramine (HMX) CAS RN: 2691-41-0 Formula: $C_4H_8N_8O_8$ FW: 296.16 Density (g/cm^3): 1.91 Source: BAE Systems, Lot No. BAE08G051	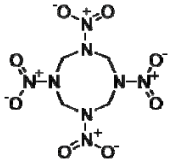
Name: Pentaerythritol tetranitrate (PETN) CAS RN: 78-11-5 Formula: $C_5H_8N_4O_{12}$ FW: 316.14 Density (g/cm^3): 1.77 Source: Ensign Bickford Primaline 21 detonating cord (100 grain/ft)	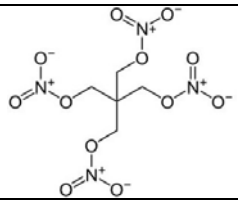
Name: Cyclotrimethylenetrinitramine (RDX) CAS RN: 121-82-4 Formula: $C_3H_6N_6O_6$ FW: 222.12 Density (g/cm^3): 1.82 Source: Ensign Bickford Primaline 21 detonating cord (100 grain/ft)	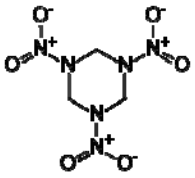
Name: Triacetone triperoxide (TATP) CAS RN: 17088-37-8 Formula: $C_6H_{12}O_4$ (Dimer) $C_9H_{18}O_6$ (Trimer) FW: 148.157 (Dimer) 222.24 (Trimer) Source: Naval Surface Warfare Center Explosive Ordnance Laboratory, Indian Head, MD: 40 mg/mL in acetone	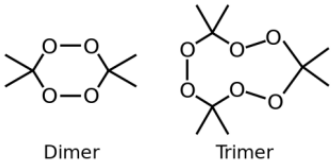 Dimer Trimer

Note: No batch/lot number was provided with the C-4 sample that had been manufactured without taggant. Batch numbers of other samples are listed in Table 5.

3 RESULTS AND DISCUSSION

3.1 Composite C (C-4)

Alone among the energetic materials studied during this project, C-4 is a composite rather than a single chemical compound. With the exception of the C-4 that had been prepared without taggant and was analyzed by ATR-VASE to determine the optical constants, the samples that are discussed in this report had been manufactured in production mode (i.e., typically 6600 lb. batches by HAAP).[18] They can vary in composition. After production, the explosive typically consists of RDX (>90% by mass of RDX), of which the RDX is described as 75% "coarse" and 25% "fine." The taggant, 2,3-dimethyl-2,3dinitrobbutane (DMDNB), which typically comprises 1-1.5% by mass of the final weight of the C-4, is added during preparation of the RDX. Following preparation of the RDX, "lacquer" is added that consists of poly(isbutylene) (PIB), machine oil, and a plasticizer. Until approximately 15 years ago, the latter component was dioctyl sebacate; production has since switched to using dioctyl adipate as plasticizer.[18] The final product typically has around 2% PIB, 2-3% oil, and 4-5% plasticizer. Oxley, et al., recently analyzed several batches of RDX that had been produced by HAAP and found that they contained 1.9-15.5% cyclotetramethylene tetranitramine (HMX) by mass.[19] This proved useful when interpreting the spectra that we obtained from the C-4.

Preparing a solution of the C-4 suitable for airbrushing, even in the absence of taggant, was challenging because of the differences in chemical properties of the various components. PIB is, for example, a fairly chemically resistant elastomer that is a primary constituent of many chemical protective ensembles (e.g., butyl rubber gloves). RDX, on the other hand, is a compound that is soluble in a variety of, primarily polar, organic solvents. After experimenting with several combinations of solvents, we found a simple method of preparing a solution consisting of approximately 50 mg/mL of C-4. Approximately 100 mg of C-4 were added to 2 mL of n-hexane (≥95%, Sigma-Aldrich; Cat. No. 650552) in a 20 mL screw cap vial. This was shaken vigorously by hand for several minutes. Thereafter, 18 mL of ACN (99.8%, Sigma-Aldrich; Cat. No. 271004) were added, and the mixture was agitated for 2 minutes at 60 Hz in a Retsch (Newtown, PA) mixer-mill.

The resulting solution, which was slightly cloudy, was decanted to the reservoir of the airbrush gun. Several milliliters of ACN were added to the screw cap vial, which was shaken by hand, and then added to the solution in the reservoir of the airbrush gun. While the solution was airbrushed onto the ZnSe crystal, the solution was shaken frequently to hinder any potential settling of particles in the mixture. After airbrushing, the resulting film was analyzed by ATR-VASE. The airbrushing and analysis by ATR-VASE was repeated a total of five times to ensure that the response (both Ψ and Δ) was stable before computing the complex optical constants. Figure 6 shows a comparison of the raw data from the C-4 (Ψ only) to the corresponding response of neat airbrushed RDX. Also seen in the figure are the final computed optical constants of the C-4. We note a small nonzero baseline effect observable in the final k spectrum; we suspect that slight scattering losses contribute to this effect. Spectral features that differentiate the C-4 from the RDX include carbonyl (C=O) stretch near 1730 cm^{-1} and C-O stretch around 1200 cm^{-1}, both of which are most likely associated with the plasticizer that is added to the RDX when the C-4 is manufactured.

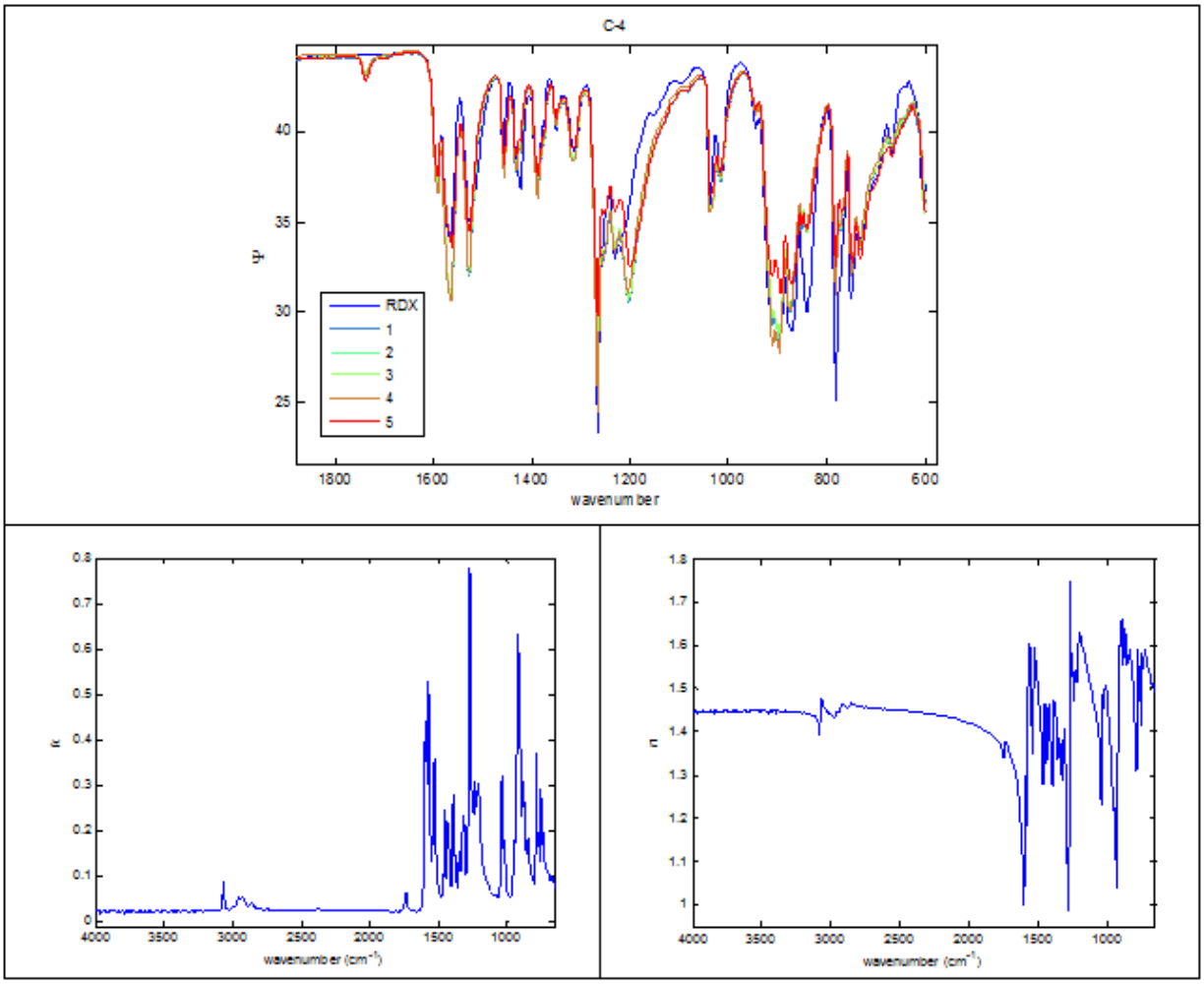

Figure 6. Top: Raw data (*Ψ*) from five repetitions of airbrushing solutions of C-4 onto ZnSe and analyzing by ATR-VASE, as well as similar data obtained from neat RDX. Bottom: Complex optical constants, *k* (left) and *n* (right) computed from the airbrushed C-4.

Table 4. Values of the optical constants of C-4 at selected points.

k		*n*	
cm^{-1}	Intensity	cm^{-1}	Intensity
752.7	0.291	614.5	1.364
785.1	0.372	747.7	1.584
923.1	0.633	755.8	1.414
1039.0	0.322	780.3	1.590
1269.9	0.778	789.9	1.309
1319.9	0.234	836.3	1.589
1391.5	0.281	872.6	1.639
1434.1	0.222	895.7	1.662
1458.0	0.246	931.8	1.039
1532.2	0.359	1011.1	1.509
1575.6	0.529	1031.0	1.488
1594.6	0.443	1043.6	1.233
		1198.2	1.630
		1265.4	1.747
		1279.6	0.987
		1308.7	1.409
		1326.1	1.287
		1347.5	1.383
		1384.3	1.473
		1397.1	1.271
		1438.7	1.328
		1453.3	1.464
		1523.4	1.595
		1538.3	1.346
		1561.8	1.604
		1582.4	1.181
		1589.8	1.299
		1603.7	1.000
		1730.9	1.375
		3998	1.447

The taggant-free sample was subjected to a fairly extensive analysis by FTIR-ATR using the Thermo-Nicolet 670 spectrometer and GoldenGate. Three aliquots of the sample were first run to examine the variations in the resulting spectra, resulting in the spectra in Figure 7. Note that no ATR correction was applied to the spectra in the figure. Compared to neat RDX (the red trace in the figure), the C-4 exhibited absorption bands associated with the PIB and plasticizer. The relative intensities of the bands arising from the binder/plasticizer varied, however. The square sample surface of the single-bounce diamond IRE is only 2 mm in diameter. The variations in the spectra in Figure 7 may give an indication of the granularity of the C-4 on that scale.

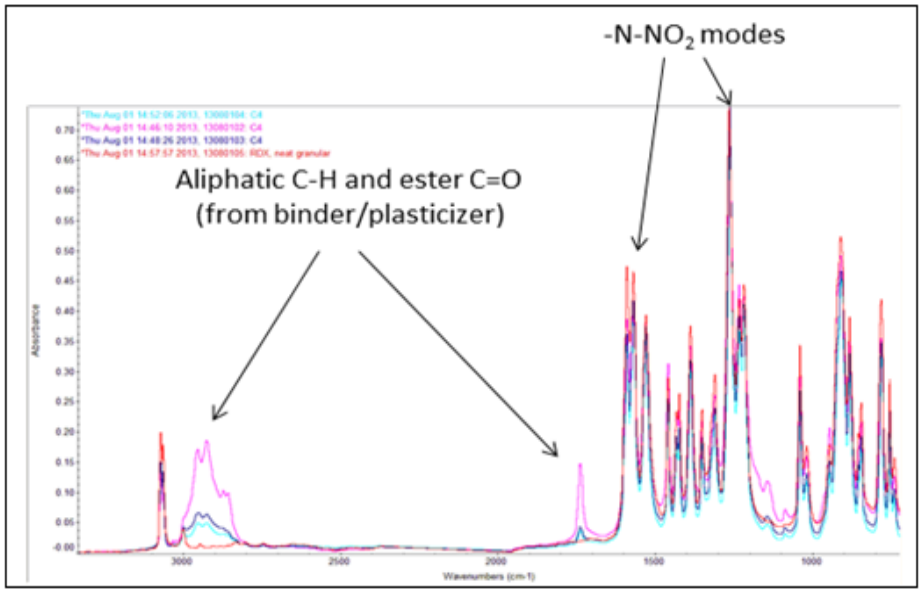

Figure 7. FTIR-ATR spectra of three aliquots of the C-4 that had been manufactured without taggant, compared to a spectrum of neat RDX (red trace). The spectra of the C-4 exhibited varying proportions of features associated with the binder and plasticizer, which are not present in the neat RDX.

The spectrum of neat RDX was scaled and subtracted from the spectrum of C-4 that exhibited the most intense features not attributable to the RDX. The resulting residual spectrum (after applying the Omnic Advanced ATR Correction) was searched using the Sigma-Aldrich Library of FTIR Spectra. Neither of the two most likely plasticizers, dioctyl adipate and dioctyl sebacate, are in the library, so a text search of the library was run using the partial compound name “adipate” to limit the search results. The closest match returned in the search was poly(1,4-butylene adipate) (PBA). Figure 8 shows the residual spectrum overlaid with the library spectrum of the PBA. Although the match between the residual spectrum and the reference PBA spectrum is certainly less than ideal, they both exhibit the strong ester carbonyl stretch (1800 to 1700 cm^{-1}) and ester C-O-C stretch (1300 to 1200 cm^{-1}). Interesting to note, however, is that only the residual spectrum has the characteristic *gem*-dimethyl doublet between 1390 to 1360 cm^{-1}, which is characteristic, in this case, of the isobutyl functionality in the PIB. The PBA structure lacks the isobutyl functional group that is present in the PIB elastomer.

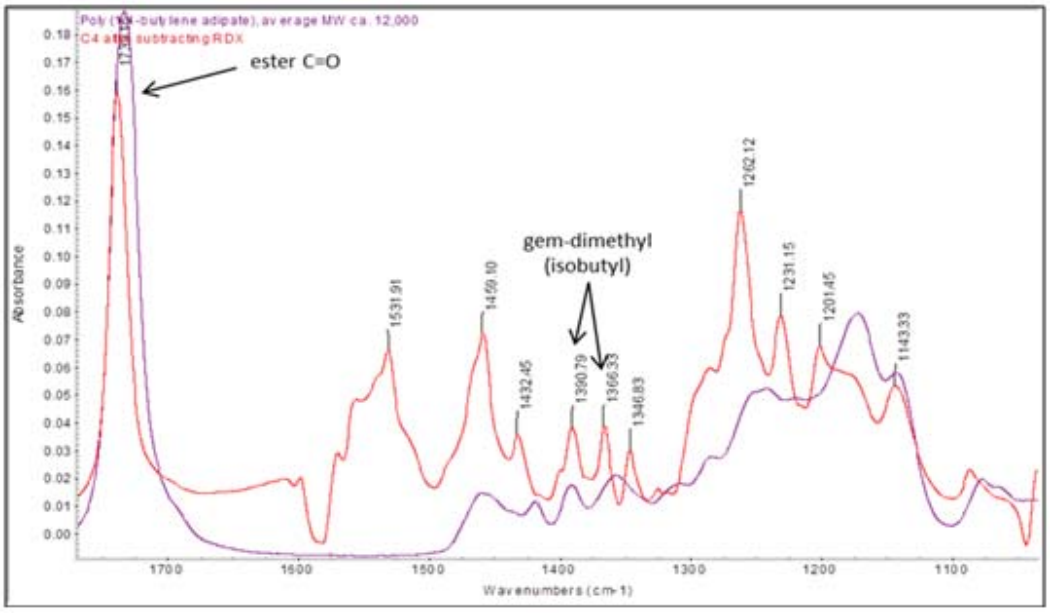

Figure 8. Spectra of C-4 after subtracting a scaled spectrum of RDX (red trace) and the spectrum of poly(isobutylene adipate), (purple trace) from the Sigma-Aldrich FTIR library. Both spectra exhibit ester C=O and C-O stretch, while only the C-4 residual spectrum has the characteristic 1390-1360 cm^{-1} doublet from the gem-dimethyl functional groups of the isobutyl in the molecular structure of the PIB.

We retained the screw cap vial in which the first sample for airbrushing had been prepared. After air drying to remove any remaining solvent, the vial was weighed, and 1 mL of hexane was then added to the vial. The vial was shaken vigorously, a few microliters of hexane were added to the IRE of the GoldenGate, and the hexane was evaporated. Figure 9 shows the resulting spectrum gave an excellent match to the library spectrum of PIB. The remaining hexane was decanted from the screw cap vial, and the vial was rinsed with multiple aliquots of polar and nonpolar organic solvents. After the vial was thoroughly rinsed and dried, it was examined visually by naked eye and with a 10x loupe to ensure no residual material remained, and the vial was reweighed. The *Δ* mass indicated that, of the 107 mg of C-4 originally added to the vial, only 1.7 mg, or 1.6% of the sample that had been prepared for airbrushing had not been either dissolved or suspended in the hexane-acetonitrile co-solvent.

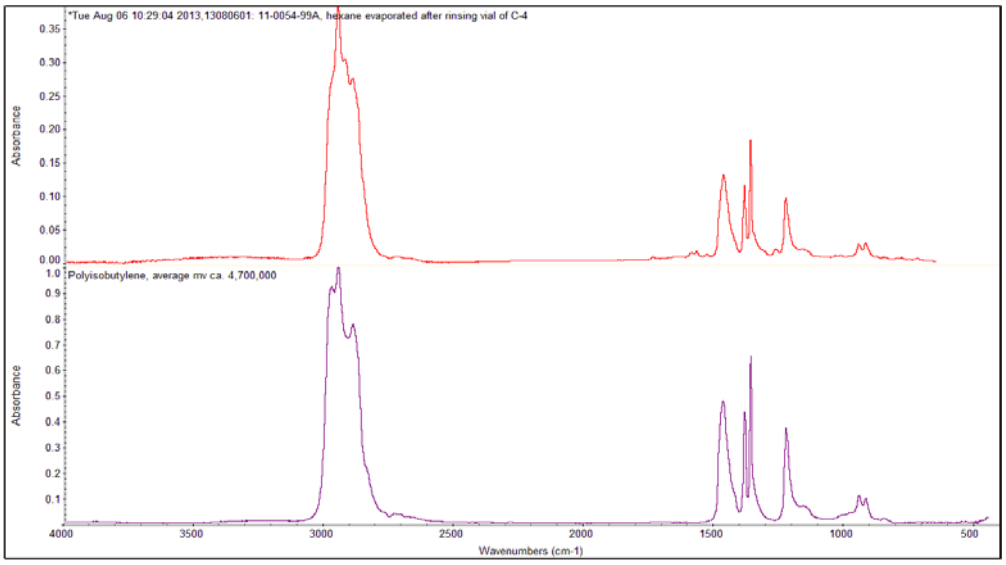

Figure 9. Spectrum of hexane extract of residual material in screw cap vial (top in red) showing an excellent match to the library spectrum of poly(isobutylene) (bottom in purple).

As noted previously, RDX manufactured by HAAP has been found to contain a mass fraction of HMX as high as 15%.[19] As seen in Table 3, the two compounds are structurally similar cyclic nitramines. This could have rendered a small mass fraction of HMX in the spectrum of the C-4 difficult to distinguish from the RDX on the basis of their spectral features. Figure 10 compares the residual spectrum of the C-4 (obtained by subtracting a scaled spectrum of RDX from the C-4) to the absorption index spectra of HMX and RDX. As the figure shows, absorption features that are unique to the HMX were observed in the residual spectrum, confirming the presence of HMX in the C-4 produced by HAAP.

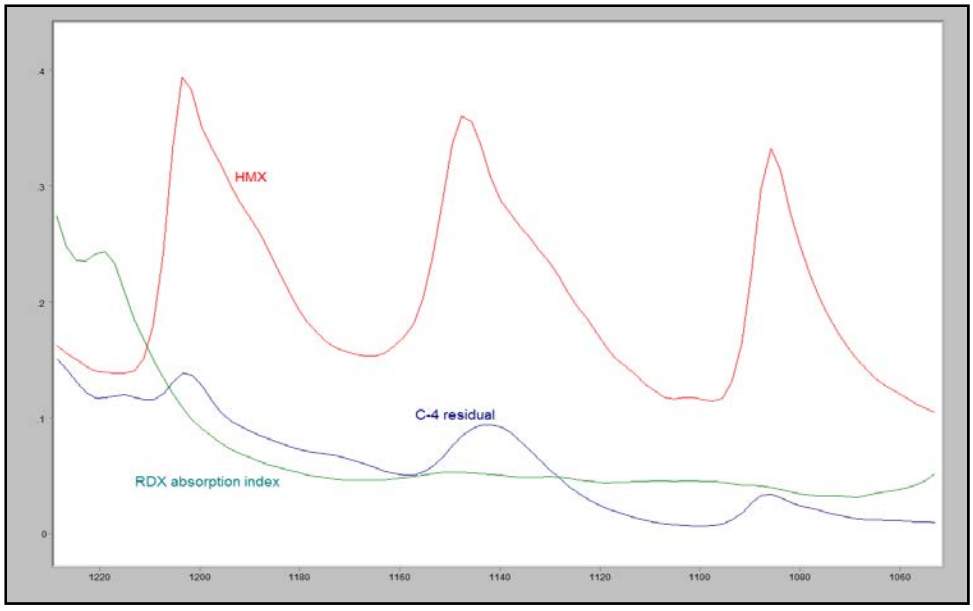

Figure 10. Absorption index spectra of HMX (red) and RDX (aqua) from ATR-VASE, and C-4 residual spectrum (RDX subtracted, dark blue). The residual spectrum exhibited features not seen in the spectrum of RDX, thus appearing to confirm the presence of HMX in the HAAP C-4.

Seven samples of C-4 manufactured by HAAP using a formulation that included DMDNB taggant were analyzed by FTIR-ATR spectrometry. Batch numbers of those samples are listed in Table 5.

Table 5. Batch numbers of C-4 that were analyzed by FTIR-ATR with the GoldenGate accessory. The samples listed were manufactured with taggant.

C-4 Batch Number
12-0022-044-01
12-0022-044-02
12-0022-044-03
12-0022-044-04
12-0022-044-05
12-0022-044-06
12-0022-044-07

The spectra of the samples of C-4 listed in Table 5 are shown in Figure 11. The mean spectrum was computed, as well as the upper and lower limits (expanded to a confidence interval of 95% using the MATLAB (Mathworks, Natick, MA) *tinv* function, which computes an inverse *Student's T* distribution). The spectra are displayed in the lower half of Figure 11.

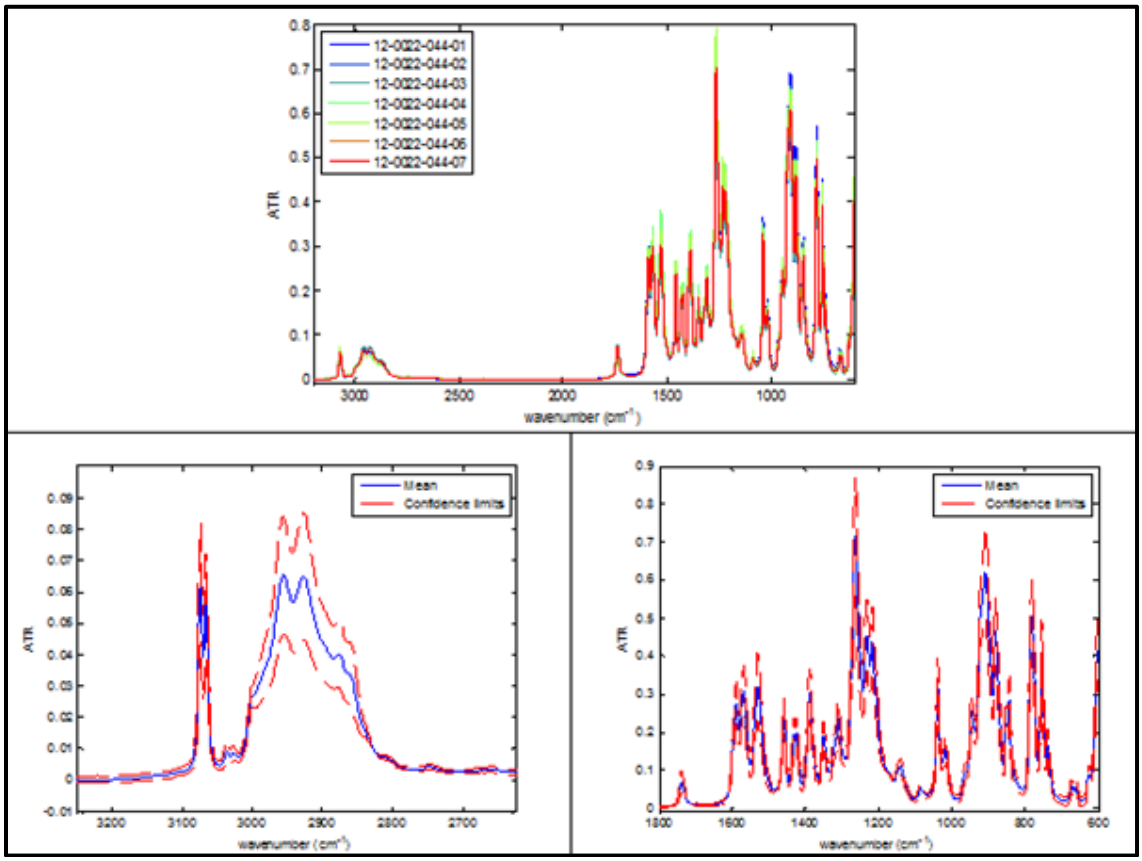

Figure 11. FTIR-ATR spectra of seven batches of C-4 manufactured with DMDNB taggant: Individual spectra with batch numbers indicated in the legend (top) and plots of mean spectrum (bottom left and right, blue trace), with confidence intervals (α = 0.05) plotted (red dotted line).

3.2 Erythritol tetranitrate (ETN)

As noted in Table 3, the airbrushed film of the ETN that was used to compute the optical constants (seen in Figure 12) was prepared from a solution at a concentration of 5 mg/mL in ACN that had been obtained from a commercial source. As seen in Table 3, ETN is a non-cyclic organic nitrate that is similar in structure to PETN. Despite the similarities in the structures of ETN and PETN, the thin films that were prepared from the two compounds were remarkably different in appearance. While the ETN was exceptionally transparent and colorless, the PETN was nearly opaque, perhaps indicating that the films had formed into different crystal morphologies.

Not surprisingly, the ETN spectrum is dominated by absorption features near 1646 cm^{-1} (the asymmetric NO_2 stretch), between 1293 and 1281 cm^{-1} (the symmetric NO_2 stretch), and near 837 cm^{-1} (the N-O stretch).[20] Several partially resolved peaks from 1057 to 1025 cm^{-1} may be associated with C-O stretch, although the most intense of these bands at 1057 cm^{-1} is slightly higher than the reported range of 1040 to 1000 cm^{-1}.[21]

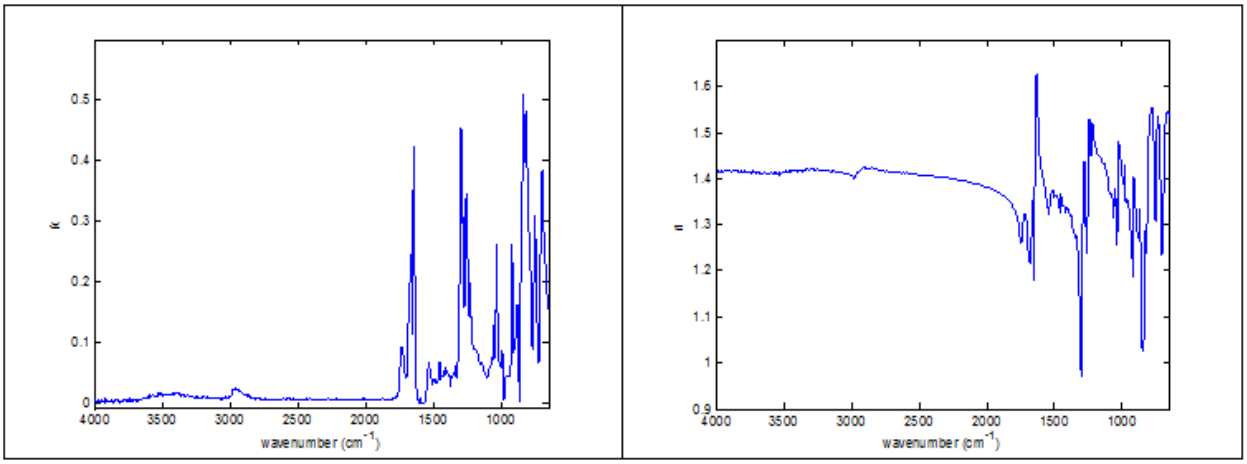

Figure 12. Computed optical constants, *k* (left) and *n* (right), of ETN from airbrushed film on ZnSe.

The non-quantitative IR spectrum of ETN was recently published by Oxley, et al.[22] The positions and relative intensities of the absorption bands were similar to the *k*-spectrum in Figure 12. Table 6 lists the values of the optical constants at selected points in the spectra.

Table 6. Values of the optical constants of ETN at selected points.

k		*n*	
cm^{-1}	Intensity	cm^{-1}	Intensity
696.9	0.384	624.9	1.546
745.1	0.280	707.0	1.233
755.1	0.310	740.4	1.537
819.5	0.484	751.5	1.491
837.1	0.510	758.4	1.305
878.3	0.162	780.4	1.554
919.2	0.260	825.6	1.237
988.5	0.085	832.2	1.287
1033.8	0.263	847.4	1.025
1059.9	0.127	873.0	1.333
1227.9	0.198	913.7	1.404
1256.2	0.347	924.4	1.187
1281.2	0.308	984.6	1.432
1293.1	0.455	1025.1	1.481
1457.1	0.067	1039.4	1.257
1536.5	0.066	1056.1	1.376
1646.2	0.425	1222.0	1.520
1663.3	0.246	1243.6	1.531
1735.0	0.092	1264.5	1.239
		1278.4	1.437
		1285.5	1.436
		1305.3	0.971
		1338.1	1.275
		1454.6	1.368
		1512.4	1.376
		1635.9	1.629
		1652.6	1.180
		1659.7	1.366
		1683.5	1.217
		1719.0	1.325
		3998	1.419

In comparison to PETN, the absorption bands associated with the NO_2 stretch were much weaker in the absorption index of ETN. This is most pronounced around the NO_2 asymmetric modes. Although both exhibit peaks with maximum intensities at 1646 cm^{-1}, ETN has k_{max}=0.425, as contrasted with PETN, which has a k_{max}=1.773. The differences in both the appearances of the airbrushed thin films and the intensities of the optical constants indicate that they appear to present optically distinct phenomena.

3.3 Hexamethylene triperoxide diamine (HMTD)

The thin film of HMTD from which the optical constants (Figure 13) were computed was prepared from a solution of the compound obtained from a commercial source at a concentration of 5 mg/mL in ACN. As with the C-4 data, some scattering losses from the crystalline films likely contribute to the slight nonzero baseline apparent in the *k* spectrum. The values of the optical constants at selected points in the spectra are listed in Table 7.

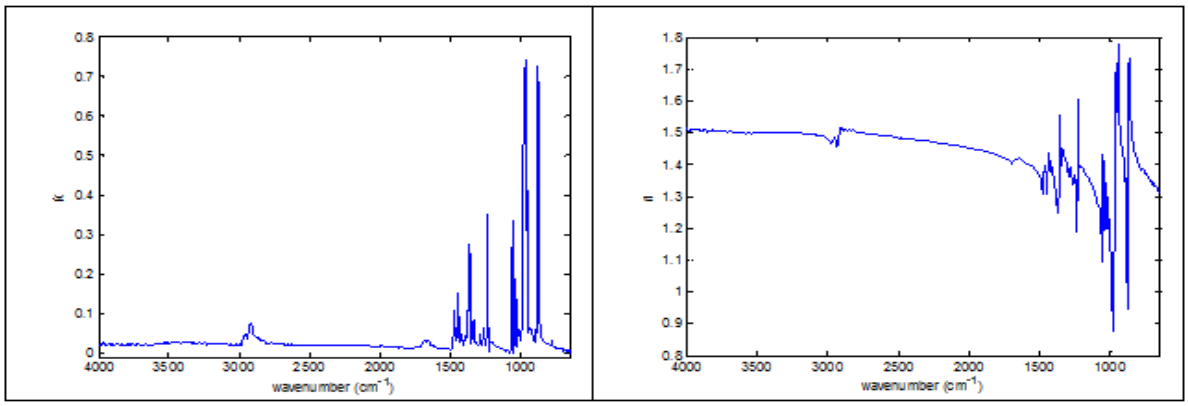

Figure 13. Computed optical constants, *k* (left) and *n* (right), of HMTD from airbrushed film on ZnSe.

Table 7. Values of the optical constants of HMTD at selected points.

k		*n*	
cm^{-1}	Intensity	cm^{-1}	Intensity
819.5	0.484	872.8	1.738
837.1	0.510	880.9	0.946
878.3	0.162	896.5	1.356
919.2	0.260	949.3	1.780
988.5	0.085	955.2	1.569
1033.8	0.263	961.4	1.694
1059.9	0.127	986.4	0.873
1227.9	0.198	1021.3	1.298
1256.2	0.347	1028.8	1.196
1281.2	0.308	1033.3	1.342
1293.1	0.455	1039.1	1.189
1457.1	0.067	1053.7	1.432
1536.5	0.066	1061.1	1.095
1646.2	0.425	1220.0	1.392
1663.3	0.246	1231.2	1.609
		1240.5	1.187
		1254.9	1.367
		1358.8	1.555
		1370.8	1.245
		1438.9	1.438
		1451.0	1.307
		1466.1	1.396
		1478.8	1.305
		3998	1.511

A comparison of the computed spectrum of HMTD (from density functional theory, DFT using Gaussian 94 and Gaussian 98) to the diffuse reflection spectrum of a single crystal of the compound has been reported in the literature by Wierzbicki and Cioffi.[23] The authors of the study were primarily interested in determining the geometry of the molecule and did not correlate either the computed or the experimental spectra to specific molecular vibrations. The experimental spectrum was obtained using a SpectraTech HATR accessory on a Nicolet 550

FTIR spectrometer. Interestingly, although the spectrum of the crystal was reported as diffuse reflection and processed using a Kubelka-Munk transform, which would have been appropriate for a diffuse reflection spectrum, the manufacturer reports that the HATR is a multi-bounce ATR accessory. This may explain, at least in part, why the computed Gaussian spectrum in the study by Wierzbicki and Cioffi, which normally should provide a better match for a gas-phase spectrum of the molecule, was more similar to our ATR-VASE *k*-spectrum than their single crystal spectrum.

A more recent study of the IR spectra of peroxide-based explosives that included HMTD and TATP was published by Schulte-Ladbeck, et al. in 2006.[24] The authors reported both FTIR-ATR and liquid chromatography-infrared (LC-IR) spectra of the compounds. Both the FTIR-ATR and LC-IR spectra of the HMTD show a better match to the k-specttrum from ATR-VASE than to the diffuse reflection spectrum reported by Wierzbicki and Cioffi.

3.4 Cyclotetramethylenetetranitramine (HMX)

HMX is a cyclic nitramine similar in structure to RDX, and the two compounds would be expected to have similar solubilities and spectral properties. We made the solution that was used to airbrush the thin film on the ZnSe crystal from HMX that had been obtained from BAE Systems (Arlington, VA; Lot No. BAE08G051). The computed optical constants are seen in Figure 14, and values of *n* and *k* at selected frequencies are listed in Table 8. These data also exhibit a small, nonzero baseline effect in what are clearly non-absorbing regions of the *k* spectrum. We deduced that this effect is likely attributed to Tyndall effect scattering by the crystalline film.

The strong, broad absorption feature near 1549 cm^{-1} is most likely associated with NO_2 asymmetric stretch. That frequency is somewhat outside of the reported range for that functional group according to one literature source,[20] although in the middle of the range reported for the functional group in energetic materials according to McNesby, et al.,[21] and specifically for HMX, according to Brand, et al.[25] The strongest absorption band in the molecule (1287 cm^{-1}), which has $k>1$, likely arises from the NO_2 symmetric stretch. A strong doublet near 950 cm^{-1} may be associated with N-O stretch, which has a reported range of 950 to 850 cm^{-1} in energetic materials,[21] although other authors assign vibrations in the spectrum of HMX in this region to the N-N-C modes.[25]

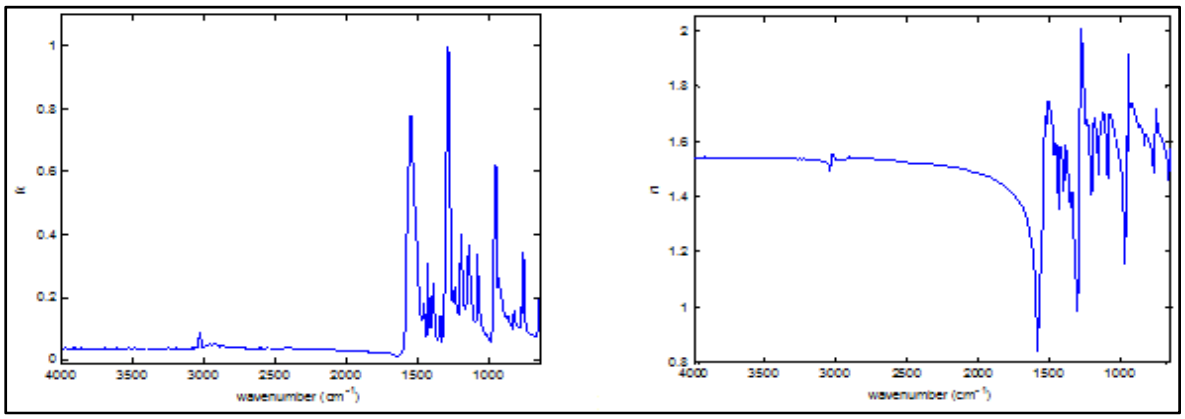

Figure 14. Computed optical constants, *k* (left) and *n* (right), of HMX from airbrushed thin film on ZnSe.

Table 8. Values of the optical constants of HMX at selected points.

k		*n*	
cm^{-1}	Intensity	cm^{-1}	Intensity
627.0	0.406	621.6	1.610
658.5	0.194	631.3	1.276
759.7	0.345	654.9	1.575
948.4	0.616	755.0	1.716
963.0	0.622	762.8	1.481
1085.4	0.341	944.8	1.918
1146.8	0.369	951.9	1.559
1202.7	0.403	957.5	1.620
1286.7	1.001	972.2	1.157
1393.8	0.249	1076.1	1.700
1431.6	0.307	1090.3	1.469
1549.4	0.780	1152.6	1.483
		1184.0	1.684
		1206.7	1.407
		1278.2	2.009
		1304.7	0.981
		1387.8	1.585
		1403.2	1.421
		1424.6	1.585
		1435.6	1.354
		1509.7	1.748
		1530.5	1.690
		1584.4	0.841
		3998	1.542

The optical constants of HMX were previously measured by Isbell, et al., using transmission measurements of the ground compound diluted in potassium bromide (KBr) and pressed in pellets, from which a K-K transformation was performed to obtain the values of the real refractive index.[26] The optical constants in the literature study are similar to those obtained by the ATR-VASE method. In particular, we noted that the maximum values of *k* found by both methods were greater than 1, which we also found for several of the other similar nitrated explosives.

3.5 Pentaerythritoltetranitrate (PETN)

As noted in Table 3, the PETN that was studied for this report had been obtained from detonating cord from Ensign Bickford Aerospace and Defense (EBAD) Company (Simsbury, CT; Part No. Primaline 21). The company is a major supplier of the material to the Department of Defense. As such, the detonating cord was certified to MIL-C-17124E and MIL-P-387C and may be considered to be “typical” military grade material. The thin film of the energetic on the ZnSe crystal was prepared by airbrushing a solution consisting of 15 mg/mL of the material dissolved in ACN (Sigma-Aldrich; Cat. No. 34998). The computed optical constants of PETN are seen in Figure 15, and values of *n* and *k* at selected frequencies are listed in Table 9.

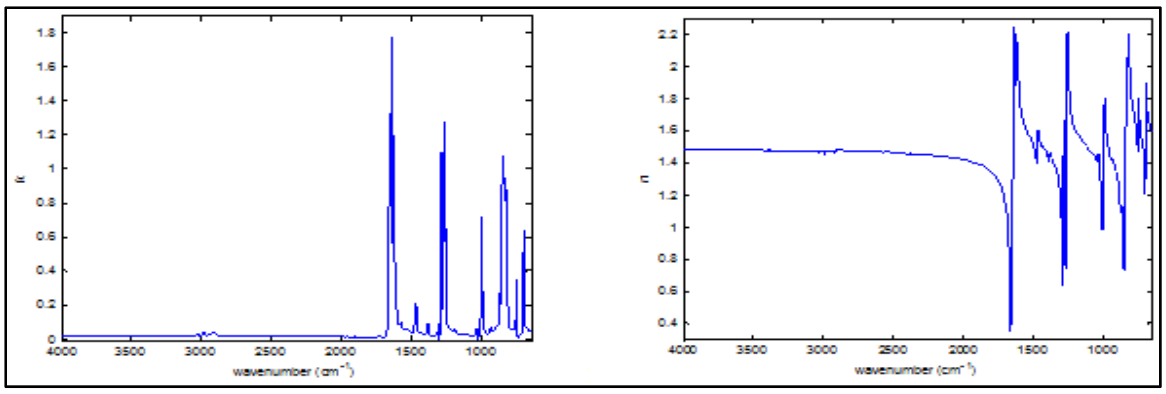

Figure 15. Computed optical constants, *k* (left) and *n* (right), of PETN from airbrushed thin film on ZnSe.

Table 9. Values of the optical constants of PETN at selected points.

k		*n*	
cm^{-1}	Intensity	cm^{-1}	Intensity
623.1	0.336	620.2	1.752
702.8	0.640	625.8	1.414
754.5	0.352	698.4	1.901
831.7	0.924	706.7	1.203
849.5	1.078	751.4	1.806
870.9	0.275	756.9	1.473
1001.6	0.715	824.2	2.197
1263.6	0.989	841.9	1.642
1270.7	1.274	857.8	0.728
1285.5	1.096	868.6	1.134
1385.6	0.087	995.6	1.797
1474.0	0.203	1006.3	0.984
1632.6	1.196	1260.2	2.206
1645.8	1.773	1265.9	1.738
		1266.9	1.811
		1274.9	0.739
		1282.5	1.658
		1289.6	0.637
		1467.7	1.604
		1479.9	1.395
		1625.3	2.206
		1635.8	1.320
		1642.0	2.242
		1663.2	0.351
		3998	1.479

To our knowledge, the complex refractive index of PETN has not been published previously. PETN can exist as ten distinct conformers, with differences in their IR spectra, as computed from density functional theory.[27-28] The literature included a qualitative spectrum of PETN obtained from a pressed pellet of the compound diluted in KBr.[27] The *k* from the ellipsometric measurement is compared to the qualitative literature FTIR spectrum in Figure 16, showing their similarity. The literature also reported the group origins of the individual vibrations

within the spectrum, based upon quantum mechanical calculations.[27-28] According to the authors of the studies, the most intense bands within the molecule (which fall within the ranges of peaks traditionally assigned to nitrogen-oxygen stretching and bending modes) probably arise primarily from these, along with contributions from other skeletal and carbon-hydrogen vibrations. Considering only the strong nitrogen-oxygen modes, the NO_2 asymmetric stretching at 1650 cm^{-1}, the NO_2 symmetric stretching at 1285 cm^{-1}, and NO stretching at 870 cm^{-1} are the dominant vibrational features in both spectra. The reference authors reported that under normal pressures, the preferred conformation of PETN crystals in S_4.[28]

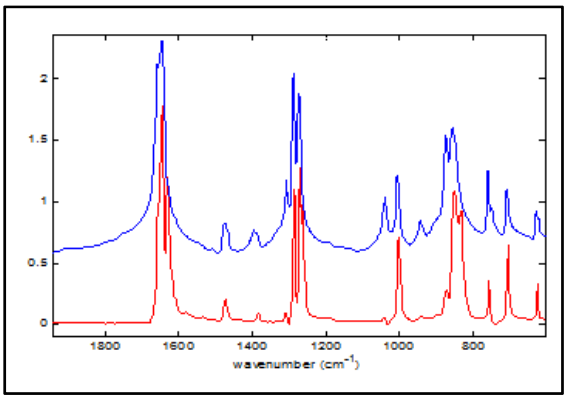

Figure 16. Comparison of the *k* from our ellipsometric measurements on PETN (red) to a non-quantitative FTIR spectrum obtained by diluting the compound in KBr and pressing it into a pellet (blue).[27] (Note: The literature spectrum was digitized, scaled, and offset for display purposes.) The two spectra exhibit similar features, with the strongest absorption bands occurring from the nitrate functional groups.

3.6 Cyclotrimethylenetrinatramine (RDX)

Similar to the PETN, the RDX that was studied for this report was cut from detonating cord that had been procured from EBAD and was certified to meet MIL-C-17124E and MIL-P-387C, and was, thus, typical military grade material. The thin film of the energetic on the ZnSe crystal was prepared by airbrushing a solution consisting of 15 mg/mL of the material dissolved in ACN. The computed optical constants of RDX are seen in Figure 17, and values of *n* and *k* at selected frequencies are listed in Table 10. We again note the presence of very slight nonzero baseline effects observable in the k spectrum.

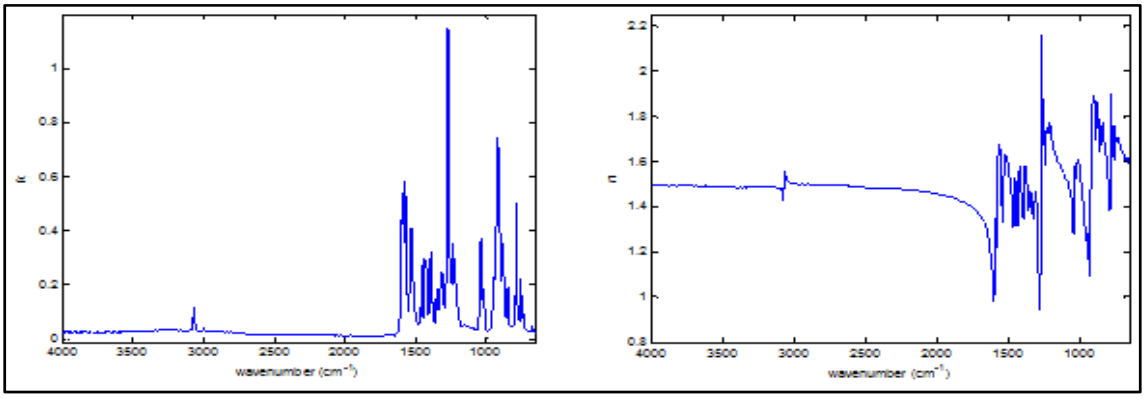

Figure 17. Computed optical constants, *k* (left) and *n* (right), of RDX from airbrushed thin film on ZnSe.

Table 10. Selected values of optical constants of RDX from ellipsometry measurements of the pressed pellet.

k		*n*	
cm^{-1}	Intensity	cm^{-1}	Intensity
753.8	0.224	611.1	1.466
785.3	0.504	757.0	1.604
845.4	0.192	780.5	1.902
881.6	0.349	789.9	1.388
923.4	0.749	841.2	1.775
1018.3	0.187	854.8	1.643
1040.0	0.372	876.2	1.863
1234.0	0.352	885.0	1.698
1268.7	1.153	900.9	1.893
1315.9	0.245	931.2	1.092
1351.2	0.187	951.1	1.244
1391.8	0.323	1010.6	1.608
1432.3	0.296	1023.1	1.523
1459.0	0.272	1034.2	1.581
1532.4	0.414	1044.2	1.281
1577.2	0.585	1238.9	1.588
1594.1	0.536	1264.6	2.162
3065.4	0.115	1279.6	0.947
3074.4	0.118	1307.6	1.473
		1325.5	1.345
		1355.7	1.378
		1385.0	1.584
		1397.1	1.343
		1420.0	1.582
		1437.8	1.317
		1455.2	1.529
		1462.7	1.310
		1522.4	1.635
		1540.1	1.330
		1565.0	1.675
		1582.8	1.218
		1589.4	1.349
		1603.5	0.982
		3067.7	1.482
		3077.6	1.424
		3998	1.496

Figure 18 shows the comparison of our measured optical constants of the thin film of RDX to the data acquired by Isbell, et al.,[26] using FTIR transmission spectroscopy. Most of the absorption bands in the two sets of optical constants are very alike in their positions and widths. There are noticeable differences as well. Most of the peaks in the extinction coefficient, *k*, from the ATR-VASE measurement of the thin film are significantly higher than in the literature spectrum. The NO_2 absorption feature at 1268 cm^{-1} is approximately twice as intense in the spectrum from the ellipsometer measurements (k_{max}=1.153) than in the FTIR transmission spectrum (k_{max}=0.578). As noted earlier in this report, the authors of the literature study found maximum values of *k* associated with NO_2 asymmetric and symmetric stretch in the spectrum of

HMX, a very similar compound, to have been greater than 1.[26] For that reason, a number of the maximum values of *k* in the spectrum of RDX that were found by the authors of the earlier study appear unusually low.

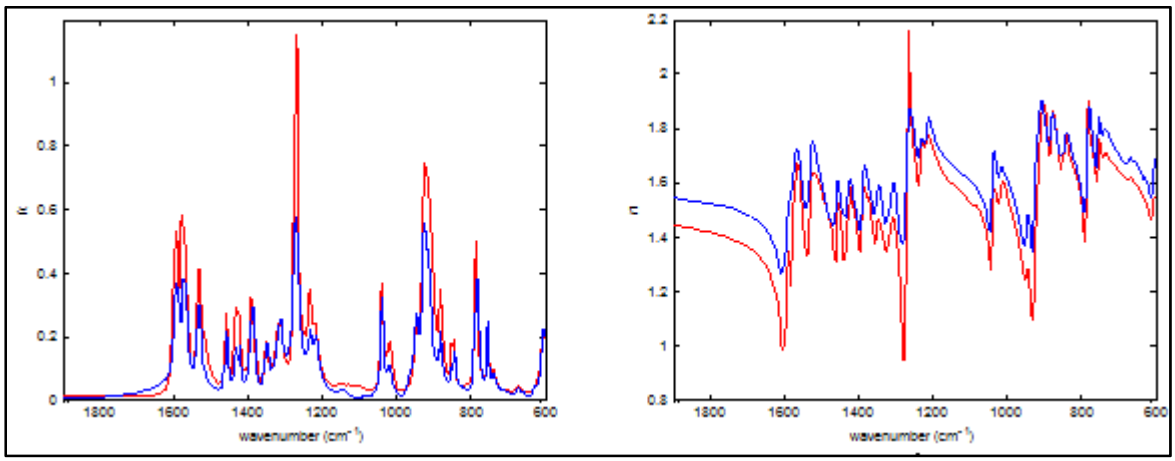

Figure 18. Comparison of the optical constants, *k* (left) and *n* (right), of ellipsometric measurements of an RDX thin film to published data obtained by FTIR transmission.[26] The literature spectra were digitized from the printed spectra.

3.7 Triacetone Triperoxide (TATP)

Although a solid, TATP has a significant vapor pressure and readily sublimates. Forming a thin film of the compound that was stable for the more than four hours necessary to acquire the spectral data to compute the optical constants proved to be challenging. Evaporating a dilute solution (5 mg/mL from Accustandard) directly onto the crystal resulted only in a thin film that sublimed almost completely before the completion of the analytical run, and the solution proved to be too dilute to achieve a thin film by airbrushing as well.

Subsequent attempts to prepare a thin film were made using a solution of the compound at a concentration of 40 mg/mL in acetone. Because acetone was not compatible with all of the plastic parts of the airbrush, we blew down the solution using dry air, and reconstituted the dry crystals in ACN to a concentration of 50 mg/mL, which was then airbrushed. In order to minimize the sublimation of the TATP in the powder cell, some of the resulting solution was evaporated onto the stainless steel body of the powder cell. The thin film was then run using the ATR-VASE. The airbrushing and analysis by ATR-VASE was repeated until the response had stabilized. The measured optical constants of the spayed TATP film are shown in Figure 1 (the black traces). The low index of refraction of the film ($n \approx 1.27$) near 4000 cm^{-1} suggested that the highly volatile TATP film still contained a non-negligible volume fraction of air at the TATP/ZnSe interface.

A 2% solution of the TATP in carbon tetrachloride was then prepared, and the solution was analyzed by ATR-VASE in a liquid cell. Thereafter, spectra of the neat carbon tetrachloride were acquired. The raw data (Ψ) from the airbrushed thin film and solutions are shown in Figure 19 and were used to acquire optical constants of both the TATP/carbon tetrachloride solution and the pure carbon tetrachloride. Those sets of optical constants could then be used to calculate the optical constants of the TATP solute using Lorentz-Lorenz effective medium approximation.[29] However, due to solvent/solute interactions, the optical constants obtained by this method often exhibit shifts in frequencies and intensities of absorption bands. We chose to

estimate the refractive index (*n*) of the TATP solution near 2200 cm^{-1} at which the absorption (*k*) is minimal. The refractive index of the TATP salute was then used to scale the optical constants of the airbrushed thin film using Maxwell-Garnett effective medium approximation[29] with the volume fraction of TATP in the airbrushed thin film as the fitting parameter. The resulting scaled optical constants of TATP are shown in Figure 20 (the red traces), and values of the optical constants at selected points are listed in Table 11.

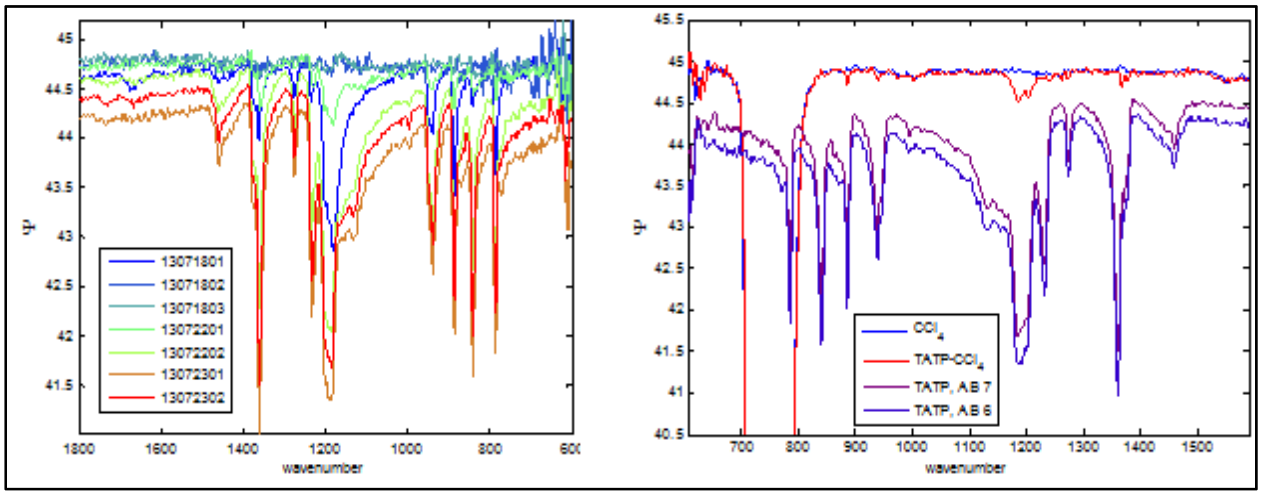

Figure 19. Raw data (*Ψ*) used to compute optical constants of TATP. (Left) Spectra of airbrushed thin filmslms of TATP. (Right) Spectra of neat carbon tetrachloride, solution of TATP in carbon tetrachloride, and last two runs from airbrushed TATP.

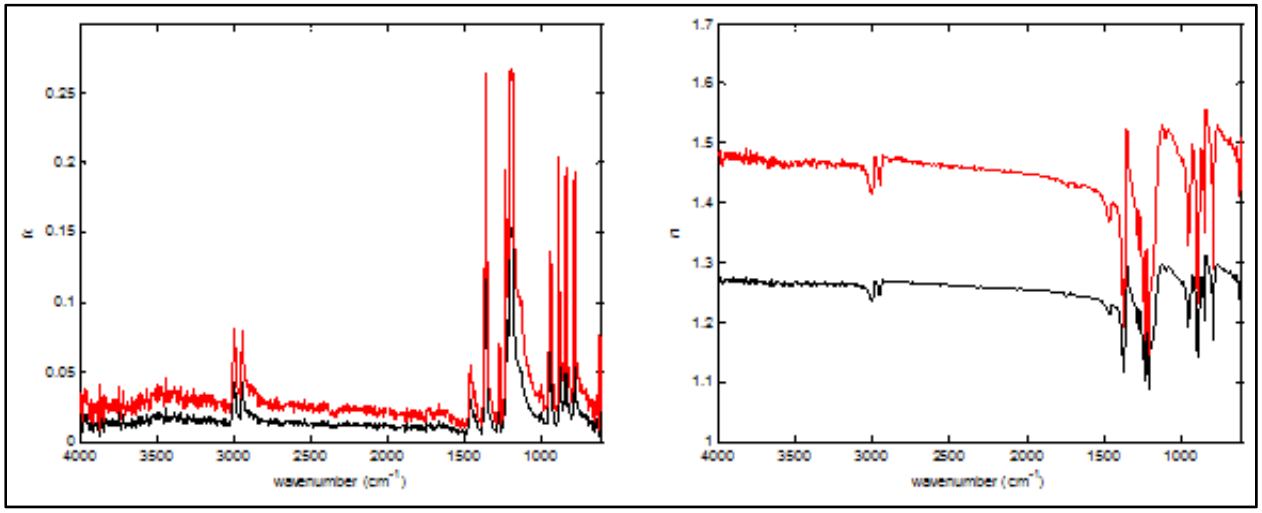

Figure 20. Computed optical constants of TATP from airbrushed thin film on ZnSe: *k* (left) and *n* (right). The black traces were computed directly from the thin film are shown; the red traces show the optical constants after scaling using the solution-phase spectra of the TATP in CCl_4.

Table 11. Selected values of optical constants of TATP from ellipsometry measurements of the pressed pellet.

k		*n*	
cm^{-1}	Intensity	cm^{-1}	Intensity
616.7	0.078	618.3	1.426
786.3	0.194	765.9	1.532
842.1	0.198	788.5	1.287
886.9	0.205	835.8	1.558
938.3	0.137	846.0	1.351
1185.0	0.266	868.3	1.492
1201.3	0.268	889.5	1.233
1231.9	0.196	928.7	1.500
1274.0	0.070	948.8	1.329
1360.6	0.264	990.4	1.476
1458.5	0.055	1121.6	1.530
2995.1	0.081	1206.4	1.148
		1225.7	1.322
		1237.1	1.171
		1269.5	1.388
		1277.6	1.323
		1353.1	1.523
		2951.6	1.427
		2983.5	1.479
		3998	1.480

To our knowledge, the IR optical constants have not previously been reported, although Schulte-Ladbeck, et al.,[24] and Oxley, et al.,[30] reported (non-quantitative) IR spectra. As a comparison, we took spectra of TATP on the Thermo-Nicolet 670 spectrometer using both the GoldenGate and an integrating sphere. As seen in Figure 21, the positions and relative intensities of the peaks in the digitized spectrum from the literature[30] and the FTIR-ATR and integrating sphere spectra are all similar to the *k*-spectrum computed from the ATR-VASE measurements. A visual examination of the spectrum from the Schulte-Ladbeck paper also showed that the positions and relative intensities of the peaks were a good match to our spectra and the spectrum from the reference literature.[30]

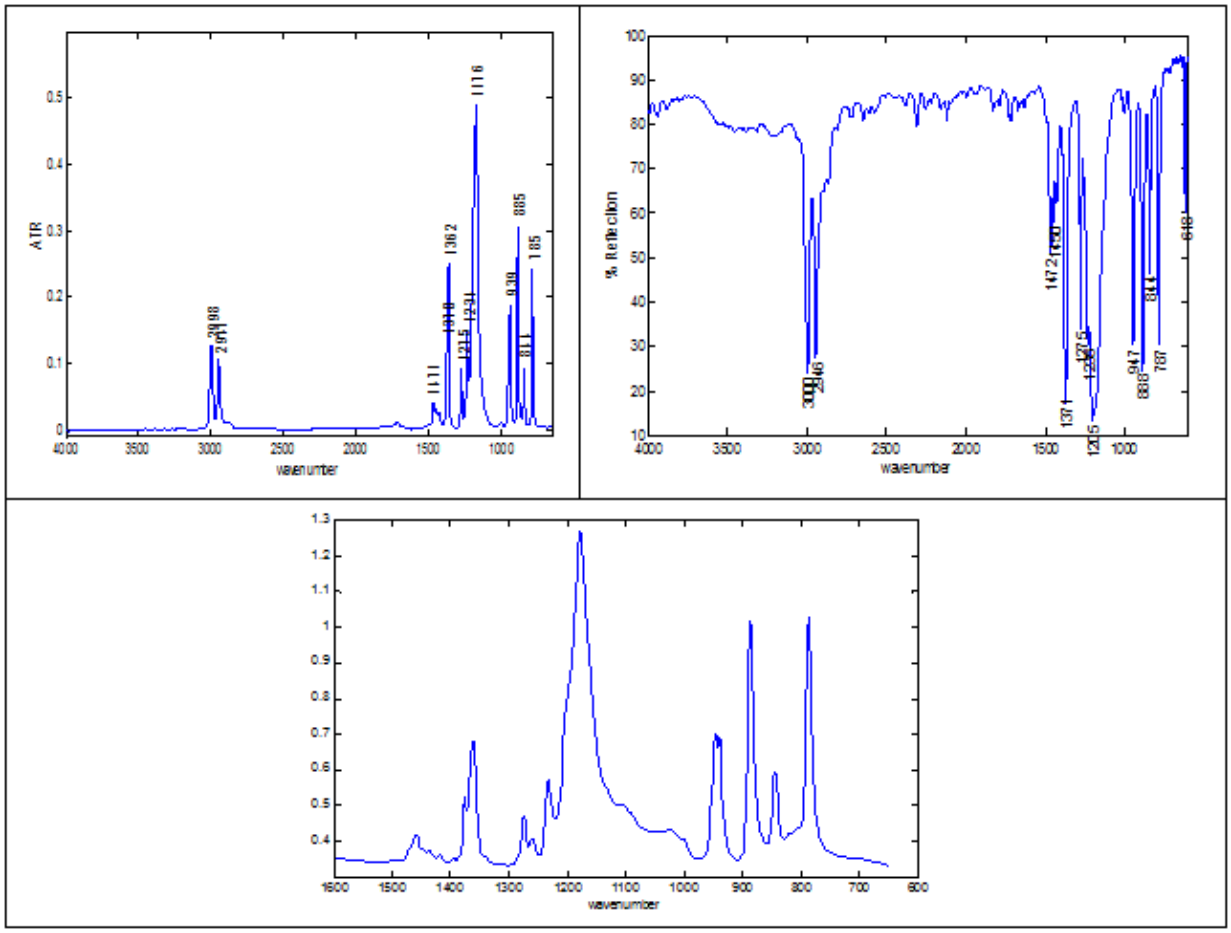

Figure 21. Top: IR spectra of TATP, with FTIR-ATR spectrum (left) and reflection spectrum from thin film acquired with an integrating sphere (right). Bottom: Spectrum digitized from the literature reference,[30] technique unknown.

4 CONCLUSIONS

We obtained the complex refractive indices of C-4, ETN, HMTD, HMX, PETN, RDX, and TATP by ATR-VASE using thin films of the materials. To our knowledge, with the exception of HMX and RDX, optical constants of these energetic materials have not previously been reported in the literature. The optical constants of HMX are similar to those reported in the literature, while the optical constants of RDX from the ATR-VASE measurements are significantly higher. Since C-4 is a composite, the ATR-VASE and the FTIR-ATR data were both recorded to reveal spectral features associated with RDX, the primary component, as well as the PIB elastomer binder and plasticizer. Absorption features were also seen in the C-4 spectra, most likely arising from HMX that was present as an impurity in the RDX. Some of the data exhibit small nonzero values of the baseline in otherwise non-absorbing regions of the *k* spectrum, presumably an unavoidable effect of scattering in the crystalline thin films. Acquiring the optical constants of TATP, which rapidly sublimes from the solid state, required a combination of measuring an airbrushed thin film of the material and then in solution phase. The results from measurements of the solution were then used to scale the response of the solid phase from the thin film measurements.

5 LITERATURE CITED

1. Hildenbrand, J.; Herbst, J.; Wöllenstein, J.; Lambrecht, A. “Explosive detection using infrared laser spectroscopy.” *Proc. of SPIE*, **7222** 72220B-1 (2009).
2. Hawranek, J.P.; Nellakantan, P.; Young, R.P.; Jones, R.N. “The control of errors in i.r. spectrophotometry – III. Transmission measurements using thin cells.” *Spectrochim. Acta*. **1976**, *32*, 75-84.
3. Hawranek, J.P.; Nellakantan, P.; Young, R.P.; Jones, R.N. “The control of errors in i.r. spectrophotometry – IV. Corrections for dispersion distortion and the evaluation of both optical constants.” *Spectrochim. Acta*. **1976**, *32*, 85-98.
4. Hawranek, J.P. and Jones, R.N. “The control of errors in i.r. spectrophotometry – V. Assessment of errors in the evaluation of optical constants by transmission measurements on thin films.” *Spectrochim. Acta*. **1976**, *32*, 99-109.
5. Wieliczka, D.M.; Weng, S.; and Querry, M.R. “Wedge shaped cell for highly absorbent liquids: infrared optical constants of water.” *Appl. Opt*., **1989**, *28*, 1714-1719.
6. Yang, C.S.C.; Williams, B.R.; Hulet, M.S.; Miles, R.W.; Samuels, A.C. *Infrared Optical Constants of GB, GF, HD, HN1, L, and VX*; ECBC-TR-1166; U.S. Army Edgewood Chemical Biological Center: Aberdeen Proving Ground, MD, **2014**; UNCLASSIFIED Report.
7. Azzam, R.M.A. and Bashara, N.M. “Generalized ellipsometry for surfaces with directional preference: Application to diffraction gratings.” *J. Opt. Soc. Am.*, **1972**, *62* 1521-1523.
8. den Boer, J.H.W.G. *Spectroscopic infrared ellipsometry: components, calibration, and application*, Ph.D. dissertation, chap.4 (University of Eindhoven, **1995**).
9. Tiwald, T.E.; Thompson, D.W.; Woollam, J.A.; and Pepper, S.V. “Determination of the mid-IR optical constants of water and lubricants using IR ellipsometry combined with an ATR cell.” *Thin Solid Film*, **1998**, *313*, 718-721.
10. Yang, C.S.C.; Williams, B.R.; Hulet, M.S.; Tiwald, T.E.; Miles, R.W.; Samuels, A.C. “Optical constants of neat liquid-chemical warfare agents and related materials measured by infrared spectroscopic ellipsometry.” *Proc. of SPIE*, **8018** 80180M-1 (**2011**).
11. Stenzel, O. *Das Dunnschichtspektrum*; Akademie Verlag: Berlin, Germany, **1996**.
12. Bertie, J.E. and Keefe, C.D. “Infrared intensities of liquids XXIV: Optical constants of liquid benzene-h6 at 25°C extended to 11.5 cm^{-1} and molar polarizabilities and integrated intensities of benzene-h6 between 6200 and 11.5 cm^{-1}.” *J. Mol. Struct.* **2004,** *695-696*, 39-57.
13. Bertie, J.E.; Apelblat, Y.; Keefe, C.D. “Infrared intensities of liquids XXV: Optical constants of liquid toluene at 25°C between 4800 and 400 cm^{-1}.” *J. Mol. Struct*. **2005**, *750*, 78-93.
14. Allara, D.L.; Baca, A.; Pryde, C.A. “Distortions of band shapes in external reflection infrared spectra of thin polymer films on metal substrates.” *Macromolecules*, **1978**, *11*, 1215-1220.
15. Graf, R.T.; Koenig, J.L.; Ishida, H. “Optical constants of thin polymer films in the infrared,” *Appl. Spectrosc.*, **1985**, *39*, 405-408.

16. Polanskiy, M., *RefractiveIndex.info*. http://refractiveindex.info (accessed December **2013**).
17. *The Aldrich Library of FT-IR Spectra*; 2nd ed.; Sigma-Aldrich: Milwaukee, WI, **1997**.
18. Jestel, Ethan A. *Holston C-4 Production Notes*; ECBC, Private communication, 9 September **2013**.
19. Oxley, J.; Smith, J.; Buco, R.; Huang , J. "A study of reduced-sensitivity RDX." *Journal of Energetic Materials*, **2007,** *25*, 141-160.
20. Colthup, N.B.; Daly, L.H.; Wiberley, S.E. *Introduction to Infrared and Raman Spectroscopy*; 3rd ed.; Academic Press: San Diego, CA, **1990**.
21. McNesby, K.L.; Pesce-Rodriguez, R.A. "Applications of vibrational spectroscopy in the study of explosives," in *Handbook of Vibrational Spectroscopy*; Chalmers, J.M. and Griffiths, P.R., Ed.; John Wiley and Sons, Ltd.: Chichester, **2002**.
22. Oxley, J.C.; Smith, J.L.; Brady, J.E.; Brown, A.C. "Characterization and analysis of tetranitrate esters." *Propellants Explos. Pyrotech.*, **2012**, *37*, 24-39.
23. Wierzbicki, A. and Cioffi, E. "Density function theory studies of hexamethylene triperoxide diamine." *J. Phys. Chem.,* **1999**, *103*, 8890-8894.
24. Schulte, R.S.; Edelmann, A.; Quintas, G.; Lendl, B.; Karst, U. "Determination of peroxide-based explosives using liquid chromatography with on-line infrared detection." *Anal. Chem.,* **2006**, *78*, 8150-8155.
25. Brand, H.V.; Rabie, R.L.; Funk, D.J.; Diaz-Acosta, I.; Pulay, P.; Lippert, T.K. "Theoretical and experimental study of the vibrational spectra of the α, β, and δ phases of octahydro-1,3,5,7-tetranitro-1,3,5,7-tetrazocine (HMX)." *J. Phys. Chem B*, **2002**, *106*, 10594-10604.
26. Isbell, R.A. and Brewster, M.Q. "Optical properties of energetic materials: RDX, HMX, AP, NC/NG, and HTPB." *Propellants, Explosives, and Pyrotechnics*, **1998,** *23*, 218-224.
27. Gruzdkov, Y.A. and Gupta, Y.M. "Vibrational properties and structure of pentaerythritol tetranitrate." *J. Phys. Chem. A*, **2001**, *105*, 6197-6202.
28. Gruzdkov, Y.A.; Dreger, Z.A.; Gupta, Y.M. "Experimental and theoretical study of pentaerythritol tetranitrate conformers." *J. Phys. Chem. A,* **2004**, *108*, 6216-6221.
29. Aspnes, D.E. "Local-field effects and effective-medium theory: A microscopic perspective." *Am. J. Phys.*, **1982**, *50*, 704-709.
30. Oxley, J.; Smith, J.; Brady, J.; Dubnikova, F.; Kosloff, R.; Zeiri, L.; Zeiri, Y. "Raman and infrared fingerprint spectroscopy of peroxide-based explosives." *Appl. Spectrosc.*, **2008**, *62*, 906-915.


EDGEWOOD CHEMICAL BIOLOGICAL CENTER
A U.S. Army RDECOM Laboratory